THE EFFECT OF WALL INERTIA ON HIGH-FREQUENCY INSTABILITIES OF FLOW THROUGH AN ELASTIC-WALLED TUBE

by MARTIN C. WALTERS

(*School of Mathematics, University of East Anglia, Norwich NR4 7TJ, UK*)

MATTHIAS HEIL

(*School of Mathematics, University of Manchester, Oxford Road, Manchester M13 9PL, UK*)

ROBERT J. WHITTAKER

(*School of Mathematics, University of East Anglia, Norwich NR4 7TJ, UK*)

Summary

We examine the effect of wall inertia on the onset of high-frequency self-excited oscillations in flow through an elastic-walled tube. The previous asymptotic model of Whittaker *et al.* (Proc. Roy. Soc. A **466**, 2010), for a long-wavelength high-frequency instability in a Starling-resistor setup, neglected inertia in the tube wall. Here, we extend this model by modifying the 'tube-law' for the wall mechanics to include inertial effects. The resulting coupled model for the fluid and solid mechanics is solved to find the normal modes of oscillation for the system, together with their frequencies and growth rates. In the system and parameter regime considered, the addition of wall inertia reduces the oscillation frequency of each mode, however its effect on the stability of the system is not as straightforward. Increasing wall inertia lowers the mean flow rate required for the onset of instability, and is therefore destabilising. However, at higher flow rates the instability growth rate is decreased, and so wall inertia is stabilising here. Overall, the addition of wall inertia decreases the sensitivity of the system to the mean axial flow rate. The theoretical results show good qualitative and reasonable quantitative agreement with direct numerical simulations performed using the oomph-lib framework.

1. Introduction

Fluid flow through elastic-walled tubes occurs in many biological systems. In the human body, the cardiovascular, respiratory and digestive systems all use flexible tubes to transport various fluids around the body. As such, the study of flows in elastic tubes is important in understanding the different phenomena that occur in these biological vessels.

In the cardiovascular system, the propagation of pulse waves in the arteries is vital for transporting blood to organs and tissues within the body. This is a well-known example, and one-dimensional models have been developed (**1**, **2**, **3**) which are able to adequately explain many properties of the system. The analysis of this problem is helped by the fact that under normal conditions the arteries have a positive transmural (internal minus external) pressure, which allows them to retain a relatively stiff, inflated state. However many blood vessels, such as the veins above the heart and outside the skull have a negative transmural pressure,

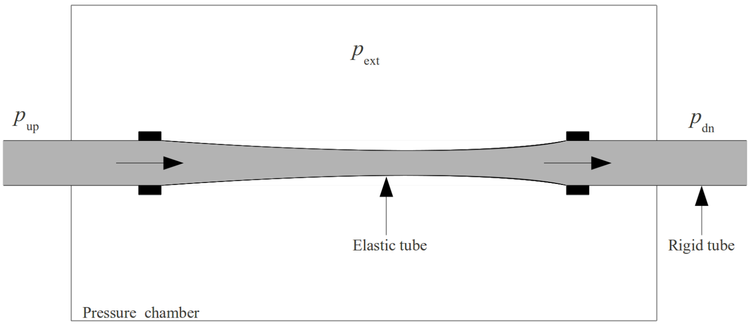

Fig. 1 The set-up of the Starling Resistor. An elastic tube is clamped between two rigid tubes and is contained in a pressure chamber with fixed pressure p_{ext}. Flow is driven through the tube using a controlled pressure difference $p_{\mathrm{up}} - p_{\mathrm{dn}}$ between the two ends. Flow can also be driven through the tube by using a volumetric pump to set a particular flux at either end. The pressure p_{ext} in the chamber can be modified to control the degree of collapse of the elastic tube.

which causes the vessels to buckle and collapse non-axisymmetrically. These vessels are much more flexible in their buckled state and small changes in fluid pressure can cause large changes in the cross-sectional area. This leads to strong interaction between the fluid and solid mechanics, which induces many interesting phenomena such as flow limitation and self-excited oscillations (**4**).

The collapse of blood vessels and the subsequent effects play an important role in many situations. For example the collapse of blood vessels is believed to be a part of the auto-regulation of blood flow to many internal organs (**5**, **6**), and the external compression of veins in lower limbs is used to prevent deep-vein thrombosis (**7**, **8**). Also, when the brachial artery is compressed by a cuff around the upper arm in blood pressure measurement, flow induced instabilities occur and "Korotkoff sounds" are generated (**9**, **10**).

Self-excited oscillations also occur in the airways and are believed to cause a number of respiratory noises. It is thought that flutter instabilities are the cause of respiratory wheezes during forced expiration (**11**, **12**), and controlled flow-induced vibrations of the vocal chords are used in speech production and can be modelled as a collapsible tube system (**13**). More examples of biological applications can be found in recent review papers (**4**, **14**, **15**).

Experimental data of fluid flow through elastic-walled tubes is usually obtained using a Starling Resistor (**16**), which is shown in Fig. 1. This comprises an elastic tube which is clamped between two rigid tubes and enclosed in a chamber with a fixed pressure. Fluid is driven through the tubes, either by applying a controlled pressure difference between the ends of the rigid tubes, or by using a volumetric pump to fix a specific flux at one end. If the transmural pressure (internal minus external) across the tube wall becomes sufficiently large and negative, the tube buckles non-axisymmetrically. Once the tube reaches this buckled state, it becomes highly compliant and small changes in the transmural pressure can cause large changes in the tube shape and cross-sectional area. Experiments by Bertram and Tscherry (**17**) have shown that if the flow exceeds a certain (set-up dependent) critical Reynolds number, the system develops self-excited oscillations. Other relevant experimental studies can be found in the review by Bertram (**18**).

Early elastic-walled-tube experiments (reviewed in (**18**)) found a vast array of different types of oscillations spanning a large range of frequencies. However, the mechanisms involved in developing self-excited oscillations are still not fully understood. Many early theoretical analyses of flow in flexible tubes were based on one-dimensional models, which are discussed in the review (**4**). Typically, these models involve terms describing three quantities: the mass flux or flow rate of the fluid within the tube, the cross-sectional area of the tube and the transmural pressure, all as functions of an axial coordinate and time. Three equations governing the quantities in the models are derived from axial momentum, mass conservation, and a 'tube law' for the wall mechanics that relates the transmural pressure to the local cross-sectional area. These kinds of models are still widely used to model networks of collapsible tubes (**19**, **20**, **21**). To be able to describe the complicated three-dimensional wall mechanics, viscous dissipation, the effects of flow separation, etc., *ad hoc* closure assumptions are required. Many of these models are able to capture qualitative effects, such as the onset of self-excited oscillations, that are observed in higher-dimensional models; see e.g. (**22**).

Pedley (**23**) introduced a model comprising a two-dimensional channel, where one wall has a segment replaced by a flexible membrane under longitudinal tension. Fluid is driven through the channel by a pressure drop between the two ends of the channel, and the transmural pressure over the membrane determines the initial shape of the membrane. Many two-dimensional models of flow through flexible tubes are based on this system, including (**24**) and (**25**). Further examples can be found in the reviews (**4**) and (**15**).

Using the system constructed by Pedley (**23**), Jensen and Heil (**26**) studied a parameter regime where the tension in the wall is large, using a combination of asymptotic analysis and numerical simulation, and determined a simple 'sloshing' instability mechanism. In this regime, the system performs high-frequency oscillations, which are governed by a dynamic balance between fluid inertia and large elastic restoring forces. The oscillations of the wall periodically displace fluid from the flexible region of the tube into the rigid regions, which results in axial sloshing flows in the rigid parts of the tube. If the amplitude of these sloshing flows is greater in the upstream rigid section than in its downstream counterpart, then there is a net influx of kinetic energy into the system. If this influx exceeds additional losses, such as viscous dissipation (most of which is found in the boundary layers near the tube walls) and work done by the pressure at the tube ends, then the system can extract energy from the flow to drive an instability. Jensen and Heil (**26**) used asymptotic techniques to obtain predictions for the frequency and growth rates of modes arising from this instability. They also found their predictions for the critical Reynolds number at which oscillations develop to be in good agreement with numerical simulations.

Whittaker *et al.* (**27**, **28**) showed that the essential components of this sloshing instability mechanism are also present in a three-dimensional flow. However, for efficient extraction of energy from the mean flow to occur, it is necessary that the tube performs oscillations about a non-axisymmetric mean state† (**29**, **27**). Hence, this instability is most likely to occur when either the tube's undeformed cross section is not circular or a tube with an initially axisymmetric cross section has buckled non-axisymmetrically. This is in agreement with

† In a tube with circular cross section, small-amplitude $O(\epsilon)$ deformations result in cross-sectional area changes and hence axial sloshing flows that are only $O(\epsilon^2)$. In contrast, with an elliptical or more general cross-section, $O(\epsilon)$ deformations will lead to larger $O(\epsilon)$ area changes and axial sloshing flows.

experimental results showing that self-excited oscillations most readily develop in tubes which are in a strongly buckled steady-state configuration (**30**).

The case where the tube has a non-circular undeformed cross section was investigated by Whittaker *et al.* (**31**), who combined models for the fluid behaviour in response to prescribed wall motion (**27**), and the wall behaviour in response to the fluid pressure in the form of a 'tube law' linking the transmural pressure with the cross-sectional area (**32**). The model in (**31**) is valid for long-wavelength, high-frequency, small-amplitude oscillations of a thin-walled, initially elliptical elastic tube under large axial tension. The predictions made by the model for the mode shapes, frequencies and growth rates of the oscillations, as well as the critical Reynolds number at which oscillations arise, were found to be in good agreement with direct numerical simulations. However, some effects such as wall inertia, axial bending, in-plane shear forces and non-linear effects in the tube wall were neglected to simplify the mathematics within the model.

In this paper, wall inertia is added to the model of Whittaker *et al.* (**31**). This is done by reintroducing the wall inertia terms to the force-balance equations governing the mechanics of the tube wall. Using the force-balance equations, a new 'tube law' is derived. Combining this with an asymptotic description of the fluid mechanics of the problem, a complete system for the interaction between the tube wall and the fluid is constructed. Solving this system, countably many oscillatory modes for the instabilities are found and their frequencies are determined. The stability criterion and growth rates of the modes of the oscillations are also determined. We find that the 'sloshing' instability mechanism (as described above) still operates. The addition of wall inertia lowers the critical axial flow rate at which the instability first appears, and increases the growth rate of the instability for moderate and low flow rates. However, at higher flow rates, the presence of the wall inertia decrease the growth rate of the instability. Hence wall inertia can act as either a destabilising or a stabilising effect, depending on the parameter values.

This paper is organised as follows. A description of the mathematical set-up used by Whittaker *et al.* (**31**) is provided in §2. In §3, we extend the work of (**32**) to derive a tube law that takes into account the inertia of the tube wall. We then combine this tube law with the fluid mechanical model of (**27**, **28**) (summarised in §4) to determine the leading-order governing ODEs for the system in §5.

In §6, we solve the system to find the frequency of the oscillations and the corresponding form of the oscillatory pressure field. It is found that, at leading order, the solutions are composed of a series of neutrally stable normal modes, each with a distinct eigenfrequency. We then quantify the effect that wall inertia has on the frequency and mode shapes of these oscillations.

In §7, we investigate the time-averaged energy budget of the system and use this to determine expressions for the (asymptotically slow) growth rates of the oscillatory normal modes. The stability boundary for each mode is expressed in the form of a critical mean-flow Reynolds number. In §8, we use these expressions to evaluate the effect of wall inertia on the stability and growth rate of each mode, and determine which mode is the most unstable and has the highest growth rate. In §9, the asymptotic predictions are compared with direct numerical simulations, and good agreement is found. Finally, conclusions are presented in §10.

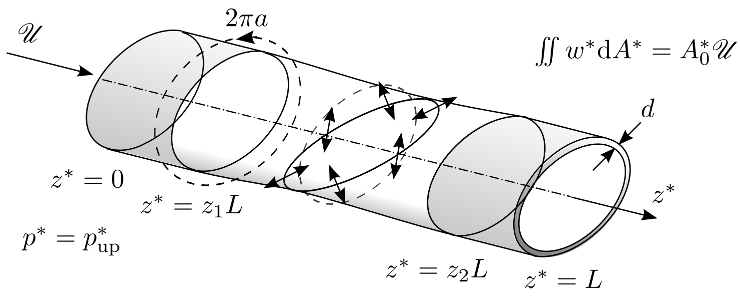

Fig. 2 The set-up used in (**31**). An initially elliptical elastic-walled tube is clamped between two rigid tubes. Fluid flows from left to right, due to a volume flux condition at the downstream end.

2. Mathematical Set-up

2.1 *Problem Description*

We adopt the same set-up as used by Whittaker *et al.* (**31**) and consider a tube of length L and circumference $2\pi a$ with an initially elliptical cross-section, as shown in Fig. 2. The tube axis is aligned with the z^*-axis and the ellipticity of the tube is set by a parameter σ_0. Using this parameter, the major and minor radii are given by $ac\cosh(\sigma_0)$ and $ac\sinh(\sigma_0)$, where

$$c = \frac{\pi \mathrm{sech}(\sigma_0)}{2\mathbf{E}(\mathrm{sech}(\sigma_0))}, \tag{2.1}$$

and $\mathbf{E}(\phi)$ is the complete elliptic integral of the second kind, defined by

$$\mathbf{E}(\phi) = \int_0^{\frac{\pi}{2}} (1 - \phi^2 \sin^2 \vartheta)^{\frac{1}{2}} \mathrm{d}\vartheta. \tag{2.2}$$

The constant c has been set so that the circumference is $2\pi a$. The cross-sectional area in the undeformed state is then

$$A_0^* = \pi a^2 c^2 \cosh(\sigma_0)\sinh(\sigma_0) = a^2 \frac{\pi^3 \tanh(\sigma_0)}{4[\mathbf{E}(\mathrm{sech}(\sigma_0))]^2}. \tag{2.3}$$

The tube is split into three regions: two rigid sections occupying $0 < z^*/L < z_1$ and $z_2 < z^*/L < 1$, and an elastic-walled section within $z_1 < z^*/L < z_2$ which is clamped onto the rigid tubes at $z^* = z_1 L, z_2 L$. The elastic section is mounted with an axial pre-stress so that in its initial elliptical configuration an axial tension force F acts at the ends, giving rise to a uniform axial pre-stress of $F/(2\pi a d)$. In its initial elliptical configuration, the elastic wall has thickness d and mass per unit area m. The elastic wall is susceptible to deformations from forces arising from the transmural (internal minus external) pressure. We assume that it behaves linearly elastically over the range of deformations we consider here, with incremental Young's modulus E and Poisson ratio ν. Using these parameters, we define the extensional stiffness D and the bending stiffness K of the tube wall as

$$D = \frac{Ed}{1-\nu^2}, \qquad K = \frac{Ed^3}{12(1-\nu^2)}. \tag{2.4}$$

Within the tube, an incompressible Newtonian fluid with density ρ and viscosity μ is driven along the tube by the imposition of a steady axial volume flux $A_0^*\mathscr{U}$ at the downstream end, $z^* = L$. At the upstream end, $z^* = 0$, the pressure is fixed at $p^* = p^*_{\mathrm{up}}$. By prescribing the flow rate at the downstream end, we ensure that no energy is lost to the mean flow there, which in turn, along with the fixed upstream pressure, ensures that the 'sloshing' instability mechanism (as described in §1) is at its most potent. Outside the tube, there is a constant external pressure p^*_{ext}, which acts on the tube wall.

As in the model of (**31**), we will consider oscillations of the fluid and tube wall with typical timescale T and amplitude $b(t^*) \ll a$, where t^* is dimensional time. The key variables we will use to describe the system are the fluid pressure p^*, the axial velocity w^* of the fluid, and the cross-sectional area A^* of the tube. In the parameter regime we shall be considering, it is found that the pressure and axial velocity are almost uniform in the tube cross-section, and the transverse velocity components do not appear at leading order.

By assuming that oscillations involve a balance between forces from the azimuthal bending of the tube wall and axial fluid inertia, we can estimate the appropriate timescale T. For this purpose, we equate the inertial pressure scale $\rho L^2 b/(aT^2)$ associated with oscillations of the fluid with the pressure scale Kb/a^4 associated with azimuthal bending of the tube wall, to obtain

$$T = \left(\frac{\rho a^3 L^2}{K}\right)^{\frac{1}{2}}. \tag{2.5}$$

2.2 *Dimensionless Groups and Parameter Regime*

We now describe the dimensionless groups involved in this problem. We first have the three geometric ratios

$$\delta = \frac{d}{a}, \qquad \ell = \frac{L}{a} \qquad \text{and} \qquad \Delta(t^*) = \frac{b(t^*)}{a}, \tag{2.6}$$

which correspond to the wall thickness, tube length and oscillation amplitude, respectively. We also have two groups related to the fluid mechanics; the Womersley number α and the Strouhal number St, defined by

$$\alpha^2 = \frac{\rho a^2}{\mu T} = \left(\frac{\rho K}{a\ell^2\mu^2}\right)^{\frac{1}{2}} \qquad \text{and} \qquad St = \frac{a}{\mathscr{U} T} = \left(\frac{K}{\rho a^3 \ell^2 \mathscr{U}^2}\right)^{\frac{1}{2}}. \tag{2.7}$$

The Womersley number represents the relative importance of unsteady inertia to viscous effects and the Strouhal number represents the relative importance of unsteady to convective inertia. Using these, we can define the Reynolds number Re as

$$Re = \frac{\rho \mathscr{U} a}{\mu} = \frac{\alpha^2}{St}. \tag{2.8}$$

Finally, we introduce a dimensionless axial tension $\mathscr{F}$ and a dimensionless wall mass M, defined by

$$\mathscr{F} = \frac{aF}{2\pi K \ell^2}, \qquad M = \frac{ma^4}{KT^2} \equiv \frac{m}{\rho a \ell^2}. \tag{2.9}$$

The dimensionless tension $\mathscr{F}$ is the ratio of the restoring forces $Fb/2\pi a L^2$ from axial tension effects to the restoring forces Kb/a^4 from azimuthal bending. The dimensionless mass M is the ratio of wall inertia forces mb/T^2 to the azimuthal bending forces Kb/a^4 or equivalently the forces $\rho ab\ell^2/T^2$ due to the fluid inertia.

As in (**31**), we consider a parameter regime where the tube wall is thin, under a large axial tension and generates small-amplitude, high-frequency, long-wavelength oscillations. We therefore have

$$\Delta(t) \ll 1, \quad \alpha \gg 1, \quad \ell St \gg 1, \quad \ell \gg 1, \quad \delta \ll 1, \quad \text{and} \quad \mathscr{F} = O(1). \tag{2.10}$$

2.3 *Non-dimensionalization*

Times are scaled on the time-scale T, transverse lengths on the radial scale a, and axial lengths on the tube length L. In particular, we introduce the dimensionless variables

$$t = \frac{t^*}{T}, \qquad z = \frac{z^*}{L}, \qquad A_0 = \frac{A_0^*}{a^2}, \qquad A = \frac{A^*}{a^2}. \tag{2.11}$$

It is assumed that the dimensionless area $A(z,t)$ varies harmonically in time with dimensionless frequency ω and amplitude $\Delta(t) = b(t)/a$. This induces an oscillatory perturbation to the axial flow, which we therefore non-dimensionalize as

$$w^* = \mathscr{U}\bar{w} + \frac{Lb}{aT}\,\mathrm{Re}\left(\tilde{w}(z)e^{\mathrm{i}\omega t}\right) + \dots, \tag{2.12}$$

where $\bar{w}$ is the steady component and $\tilde{w}$ is the (possibly complex) z-dependent amplitude of the oscillatory component. The scale for the steady flow comes from the imposed flux $A_0^*\mathscr{U}$ at the downstream end. The scale for the oscillatory perturbation arises from the continuity equation, given the amplitude and geometry of the wall motion. As discussed in §4 below, the high frequency and large aspect ratio of the system results in the leading-order oscillatory axial velocity $\tilde{w}$ being uniform in the cross-section of the tube.

This axial flow must be driven by a pressure gradient. Thus a similar form is required for the fluid pressure p^*, with both steady and oscillatory components. We write

$$p^* - p^*_{\mathrm{up}} = \frac{\mu L\mathscr{U}}{a^2}\bar{p} + \frac{\rho L^2 b}{aT^2}\,\mathrm{Re}\left(\tilde{p}(z)e^{\mathrm{i}\omega t}\right) + \dots, \tag{2.13}$$

where $\bar{p}$ is the steady component and $\tilde{p}$ is the amplitude of the oscillatory component. The steady component has been non-dimensionalized using the viscous scale $\mu L\mathscr{U}/a^2$, while for the oscillatory component we use the inertial scale $\rho L^2 b/aT^2 \equiv \Delta K/a^3$.

The steady external pressure p^*_{ext} and the transmural pressure $p^*_{\mathrm{tm}} = p^* - p^*_{\mathrm{ext}}$ are non-dimensionalized as

$$p^*_{\mathrm{ext}} - p^*_{\mathrm{up}} = \frac{\mu L\mathscr{U}}{a^2}\bar{p}_{\mathrm{ext}}, \qquad p^*_{\mathrm{tm}} = \frac{K}{a^3}p_{\mathrm{tm}}, \tag{2.14}$$

based on the the viscous scale and the azimuthal bending scale respectively. Combining these with the expression (2.13) for the fluid pressure p^*, we find that the non-dimensional transmural pressure p_{tm} can be written as

$$p_{\mathrm{tm}} = \frac{1}{\alpha^2\ell St}(\bar{p} - \bar{p}_{\mathrm{ext}}) + \Delta(t)\,\mathrm{Re}\left(\tilde{p}(z)e^{\mathrm{i}\omega t}\right) + \dots. \tag{2.15}$$

The components of the transmural pressure will act to deform the tube wall, causing both steady and oscillatory changes in the cross-sectional area. The respective scales are determined by balancing the azimuthal bending forces with the transmural pressure, and we write

$$A(z,t) = A_0 + \frac{1}{\alpha^2 \ell St}\bar{A}(z) + \Delta(t)\,\mathrm{Re}\left(\tilde{A}(z)e^{\mathrm{i}\omega t}\right) + \ldots, \tag{2.16}$$

where A_0 is the cross-sectional area in the undeformed state, $\bar{A}(z)$ is the change in area due to the steady component of the transmural pressure, and $\tilde{A}(z)$ is the axial mode shape of the change in area due to the oscillations of the wall.

Energy and energy fluxes are non-dimensionalized using

$$\rho \mathscr{U}^2 a^2 L \qquad \text{and} \qquad \rho \mathscr{U}^3 a^3. \tag{2.17}$$

These are based on the kinetic energy and kinetic energy fluxes in the steady flow.

The mid-plane of the tube wall is parameterized with dimensional Lagrangian coordinates (x^1, x^2), which are measures of arc length in the azimuthal and axial directions respectively, in the undeformed state.† We also introduce two dimensionless Lagrangian surface coordinates, $\tau \in [0, 2\pi)$ and $z \in [0,1]$. Following Whittaker *et al.* (**32**), these are related to (x^1, x^2) by $\mathrm{d}x^1 = ah(\tau)\mathrm{d}\tau$ and $\mathrm{d}x^2 = a\ell \mathrm{d}z$, where

$$h(\tau) = c(\sinh^2(\sigma_0) + \sin^2\tau)^{\frac{1}{2}} = c\left(\frac{1}{2}\cosh 2\sigma_0 - \frac{1}{2}\cos 2\tau\right)^{\frac{1}{2}}, \tag{2.18}$$

is the scale factor when (σ_0, τ) are considered to be elliptical polar coordinates.

Using the dimensionless surface coordinates, the position $\mathbf{r}$ of the wall mid-plane in the deformed state is defined as

$$\mathbf{r} = \mathbf{r}_0(\tau, z) + \frac{a}{h(\tau)}\left(\xi(\tau,z,t)\hat{\mathbf{n}} + \eta(\tau,z,t)\hat{\mathbf{t}}\right) + a\ell\left(\frac{1}{\ell^2}\zeta(\tau,z,t) + \delta^2\zeta_a(z,t)\right)\hat{\mathbf{z}}. \tag{2.19}$$

Here, $\mathbf{r}_0$ is the initial position of the surface element and the vectors $\hat{\mathbf{n}}$, $\hat{\mathbf{t}}$ and $\hat{\mathbf{z}}$ are unit vectors in the normal, azimuthal and axial directions of the undeformed tube, respectively. We have also introduced the $O(1)$ dimensionless functions $\xi(\tau,z,t)$ and $\eta(\tau,z,t)$ to represent the normal and tangential displacements of the wall, as well as the dimensionless functions $\zeta_a(z,t)$ and $\zeta(\tau,z,t)$ to represent components of the axial displacements‡. The scalings of the terms within (2.19) are based on the sizes of the deformations found in (**32**).

3. A Tube Law to Model the Wall Mechanics

3.1 *Momentum equations*

Starting from the Kirchhoff–Love shell equations (**33**, **34**), Whittaker *et al.* (**32**) derived leading-order equilibrium equations for the tube wall in the normal, azimuthal and axial directions. Using the assumptions of small-amplitude, long-wavelength perturbations of a thin-walled tube, Whittaker *et al.* were able to express the equilibria in terms of a dimensionless azimuthal hoop stress $\tilde{N}(\tau,z,t)$, an in-plane shear stress $\tilde{S}(\tau,z)$, and the displacement functions $\xi(\tau,z,t)$, $\eta(\tau,z,t)$, $\zeta_a(z,t)$ and $\zeta(\tau,z,t)$.

† Note that the superscripts denote coordinate directions and are not to be mistaken for powers.

‡ Two functions are needed because the azimuthally averaged axial displacement ζ_a has a different scaling from the azimuthally varying zero-azimuthal-mean component ζ.

To these equilibrium equations, we add the appropriate inertia terms, arising from the components of $m\ddot{\mathbf{r}}$, non-dimensionalized by the transmural pressure scale K/a^3 from (2.14). The resulting equations (which differ only by the addition of the terms involving M) are

$$\bar{B}\tilde{N} + \frac{\mathscr{F}}{h}\frac{\partial^2 \xi}{\partial z^2} - \frac{1}{h}\frac{\partial}{\partial \tau}\left(\frac{1}{h}\frac{\partial}{\partial \tau}\left(\frac{\beta}{h}\right)\right) + p_{\rm tm} + \frac{M}{h}\ddot{\xi} = 0, \tag{3.1}$$

$$\frac{1}{h}\frac{\partial \tilde{N}}{\partial \tau} + h\frac{{\rm d}\tilde{S}}{{\rm d}z} + \frac{\mathscr{F}}{h}\frac{\partial^2 \eta}{\partial z^2} + \frac{\bar{B}}{h}\frac{\partial}{\partial \tau}\left(\frac{\beta}{h}\right) + \frac{M}{h}\ddot{\eta} = 0, \tag{3.2}$$

$$\frac{1}{\ell}\frac{\partial}{\partial z}\left(\nu\tilde{N} + 12(1-\nu^2)\left(\frac{1}{\delta^2\ell^2}\frac{\partial \zeta}{\partial z} + \frac{d\zeta_a}{dz}\right)\right) + \mathscr{F}\ell\frac{\delta^2}{12}\frac{\partial \tilde{N}}{\partial z}$$
$$+\mathscr{F}\ell(2-\nu)\left(\frac{1}{\ell^2}\frac{\partial^2\zeta}{\partial z^2} + \delta^2\frac{d^2\zeta_a}{dz^2}\right) + M\ell\left(\frac{1}{\ell^2}\ddot{\zeta} + \delta^2\ddot{\zeta}_a\right) = 0, \tag{3.3}$$

where

$$\bar{B} = -\frac{c^2\sinh(2\sigma_0)}{2h^3}, \qquad \beta = -\frac{2}{c^2\sinh(2\sigma_0)}\frac{\partial}{\partial \tau}\left(1 + \frac{\partial^2}{\partial \tau^2}\right)\eta, \tag{3.4}$$

are the base-state azimuthal curvature and the azimuthal curvature perturbation respectively.

In the normal direction (3.1), the terms arise from azimuthal base-state curvature times hoop stress, base-state axial tension times axial curvature, azimuthal bending, transmural pressure, and normal inertia, respectively. In the azimuthal direction (3.2), the terms arise from hoop stress variation, in-plane shear variation, base-state axial tension times in-plane axial curvature, base-state curvature times azimuthal curvature perturbation variation, and azimuthal inertia, respectively. In the axial direction (3.3), the terms arise from axial stress variation, base-state axial tension times hoop stress variation, base-state axial tension times axial stretching variation, and axial inertia, respectively.

Whittaker *et al.* (**32**) found that $\tilde{S}(\tau, z)$ depends only on z at leading order, and for perturbations that do not involve an axial twist, that leading-order component is zero. The hoop stress $\tilde{N}$ involves contributions from ξ, η and ζ, but can be eliminated between (3.1) and (3.2) to obtain a system involving just ξ and η. Finally, it was shown in (**32**) that the asymptotic thinness of the shell enforces a geometrical constraint of negligible azimuthal stretching. This implies

$$\xi\bar{B} + \frac{\partial}{\partial \tau}\left(\frac{\eta}{h}\right) = 0 \tag{3.5}$$

at leading order, which allows ξ to be eliminated in favour of η. We thus arrive at a single partial differential equation for $\eta(\tau, z)$:

$$\mathscr{L}(\mathscr{K}(\eta)) - \mathscr{F}\frac{\partial^2}{\partial z^2}\mathscr{J}(\eta) + M\mathscr{J}(\ddot{\eta}) = p_{\rm tm}(z,t)C_p h, \tag{3.6}$$

where $\mathscr{L}$, $\mathscr{K}$ and $\mathscr{J}$ are differential operators in τ and $C_p(\tau)$ is a known function. Expressions for each of these can be found in Appendix A. The fact that the same operator $\mathscr{J}$ appears in both the $\mathscr{F}$ and M terms in (3.6) is a consequence of the $\mathscr{F}\,\partial^2/\partial z^2$ and $M\,\partial^2/\partial t^2$ terms appearing in the same way in (3.1) and (3.2). Once a solution to (3.6) for $\eta(\tau, z)$ has been found, $\xi(\tau, z)$ can be recovered from (3.5), and $\zeta_a(z, t)$ and $\zeta(\tau, z, t)$ from (3.3).

3.2 *The Tube Law*

We represent the azimuthal displacement η as a Fourier series in the azimuthal coordinate τ:

$$\eta(\tau, z, t) = \sum_{n=1}^{\infty} e_n(z,t)\,\sin(2n\tau)\,. \tag{3.7}$$

By using (2.19) and (3.5), it may be shown that the change in cross-sectional area is then given, to leading order, by

$$A(z,t) - A_0 = \frac{1}{a^2}\int_0^{2\pi a} (\mathbf{r}-\mathbf{r}_0)\cdot\hat{\mathbf{n}}\,\mathrm{d}x^1 = \int_0^{2\pi} \xi(z,\tau,t)\,\mathrm{d}\tau = \frac{6A_0\,e_1(z,t)}{c^2\sinh^2(2\sigma_0)}\,. \tag{3.8}$$

It was shown in (**32**) that when $M=0$ solutions to (3.6) are dominated by the $n=1$ component of the Fourier expansion (3.7). Since the additional inertia term takes the same azimuthal form $\mathscr{J}$ as the axial tension term, we assume this result holds true in our case too.

Projecting (3.6) on to the first Fourier mode and using (3.8) to replace e_1 by $A - A_0$, we arrive at

$$p_{\text{tm}}(z,t) = \frac{k_0}{A_0}(A(z,t)-A_0) - \frac{k_2\mathscr{F}}{A_0}\frac{\partial^2 A(z,t)}{\partial z^2} + \frac{k_2 M}{A_0}\frac{\partial^2 A(z,t)}{\partial t^2}. \tag{3.9}$$

where $k_0(\sigma_0)$ and $k_2(\sigma_0)$ are the numerically determined $O(1)$ constants found by (**32**) from the corresponding calculation when $M=0$. Equation (3.9) is the new tube law relating the transmural pressure p_{tm} to the changes in cross-sectional area A of the tube.

As this tube law is linear, we can decompose it into steady and oscillatory components. Applying (2.15) and (2.16), the steady and oscillatory components of (3.9) are found to be

$$\bar{p} - \bar{p}_{\text{ext}} = \frac{k_0}{A_0}\bar{A}(z) - \frac{k_2\mathscr{F}}{A_0}\frac{\mathrm{d}^2\bar{A}(z)}{\mathrm{d}z^2}, \tag{3.10}$$

$$\tilde{p}(z) = \frac{k_0}{A_0}\tilde{A}(z) - \frac{k_2\mathscr{F}}{A_0}\frac{\mathrm{d}^2\tilde{A}(z)}{\mathrm{d}z^2} - \frac{k_2 M\omega^2}{A_0}\tilde{A}(z). \tag{3.11}$$

We note that the steady component (3.10) of the tube law is the same as that derived in (**31**). However, the oscillatory component (3.11) now has an extra term arising from the wall inertia.

4. Fluid Mechanics

We now consider the fluid mechanics of the system. The fluid velocity $\mathbf{u}^*$ and pressure p^* are governed by the Navier-Stokes equations (**35**):

$$\rho\left(\frac{\partial\mathbf{u}^*}{\partial t} + \mathbf{v}\cdot\nabla\mathbf{u}^*\right) = -\boldsymbol{\nabla}p^* + \mu\nabla^2\mathbf{u}^*, \tag{4.1}$$

$$\nabla\cdot\mathbf{u}^* = \mathbf{0}, \tag{4.2}$$

together with no-slip conditions on the tube wall, and the appropriate pressure or flux conditions at the tube ends.

In our model, only the axial components of the velocity contribute at leading order.

Whittaker *et al.* (**27**) showed that at leading order the flow can be decomposed into steady and oscillatory components, and also that the leading-order steady component $\bar{w}$ of the axial velocity is not altered by the $O((\alpha^2 \ell St)^{-1}, \Delta)$ displacements of the tube wall. Thus, at leading order, $\bar{w}$ is given by three-dimensional Poiseuille flow in the elliptical undeformed configuration. As the extra wall-inertia terms included here only affect the wall mechanics and not the fluid mechanics, the steady component $\bar{w}$ of the axial velocity has the same form at leading order in this model. The precise solution for $\bar{w}$ is not needed for the following analysis, and so is omitted here.

In turn, the steady component $\bar{p}$ of the pressure also takes the same form as that found in (**27**) — an $O(1)$ viscous component and an $O(\alpha^2 \ell St \Delta^2)$ component induced by nonlinear Reynolds stresses from the oscillatory flow. This latter component is much smaller for the numerical simulations detailed in §9 below and so is neglected here. With the viscous component only, we have

$$\bar{p}(z) = -\bar{G}z, \tag{4.3}$$

where

$$\bar{G} = \frac{16 \cosh 2\sigma_0}{c^2 \sinh^2 2\sigma_0}. \tag{4.4}$$

Using a long-wavelength approximation and the property that the oscillatory component of the axial velocity has a high frequency, Whittaker *et al.* (**27**) showed, at leading order, that the oscillatory axial velocity $\tilde{w}$ has a plug flow profile in the core, with passive viscous boundary layers (Stokes layers) near the wall, and also that the oscillatory pressure $\tilde{p}$ is uniform in each cross-section. Hence, we have $\tilde{w} = \tilde{w}(z)$, $\tilde{p} = \tilde{p}(z)$ in the core. With these forms, the leading-order oscillatory components of the continuity and axial momentum equations are

$$A_0 \frac{\mathrm{d}\tilde{w}}{\mathrm{d}z} + \mathrm{i}\omega \tilde{A} = 0, \tag{4.5}$$

$$\mathrm{i}\omega \tilde{w} = -\frac{\mathrm{d}\tilde{p}}{\mathrm{d}z}. \tag{4.6}$$

By eliminating $\tilde{w}$ between (4.5) and (4.6), the following relationship between $\tilde{p}$ and $\tilde{A}$ is obtained:

$$\tilde{A} = -\frac{A_0}{\omega^2} \frac{\mathrm{d}^2 \tilde{p}}{\mathrm{d}z^2}. \tag{4.7}$$

5. Combined System for Fluid-Structure Interaction

We now combine the description of the wall mechanics in §3 with the description of the fluid mechanics in §4.

5.1 *Steady Area Variation*

The steady component (3.10) of the tube law may be combined with the expression (4.3) for the steady component $\bar{p}$ of the pressure to yield an ODE for the steady component $\bar{A}$ of the area variation. By noting that there is no area variation within the rigid parts of the tube situated at $0 < z < z_1$ and $z_2 < z < 1$, it is seen that we also have the boundary conditions

$\bar{A}(z_1) = \bar{A}(z_2) = 0$. Solving the ODE for $\bar{A}$ and applying these boundary conditions, the solution for $\bar{A}$ in the collapsible region $z_1 < z < z_2$ is found to be

$$\frac{\bar{A}}{A_0} = -\frac{(\bar{G}z_1 + \bar{p}_{\mathrm{ext}})}{k_0}\left[1 - \frac{\cosh\left(\kappa\left(\mathscr{Z} - \frac{1}{2}\right)\right)}{\cosh\left(\frac{1}{2}\kappa\right)}\right] - \frac{\bar{G}(z_2 - z_1)}{k_0}\left[(1 - \mathscr{Z}) - \frac{\sinh\left(\kappa\left(1 - \mathscr{Z}\right)\right)}{\sinh(\kappa)}\right], \tag{5.1}$$

where

$$\kappa^2 = \frac{k_0(z_2 - z_1)^2}{k_2\mathscr{F}}, \qquad \mathscr{Z} = \frac{z_2 - z}{z_2 - z_1}, \tag{5.2}$$

and $\bar{G}$ is given by (4.4). It is noted that $\bar{A} = O(1)$ implies an $O(\alpha^{-2}\ell^{-1}St^{-1})$ perturbation to the dimensionless cross-sectional area A.

5.2 *The Oscillatory Perturbation*

Using the oscillatory component (3.11) of the tube law obtained from the wall mechanics and the relation (4.7) derived from the fluid mechanics, we now form the governing ODEs for the self-excited oscillations of the system within each section of the tube. Eliminating $\tilde{A}$ between (3.11) and (4.7), we obtain the following for flow inside the flexible region of the tube:

$$k_2\mathscr{F}\frac{\mathrm{d}^4\tilde{p}}{\mathrm{d}z^4} + (M\omega^2 k_2 - k_0)\frac{\mathrm{d}^2\tilde{p}}{\mathrm{d}z^2} - \omega^2\tilde{p} = 0, \quad \text{for} \quad z_1 < z < z_2. \tag{5.3}$$

In the rigid sections of the tube we have $\tilde{A} = 0$, and so (4.7) implies

$$\frac{\mathrm{d}^2\tilde{p}}{\mathrm{d}z^2} = 0, \quad \text{for} \quad 0 < z < z_1 \quad \text{and} \quad z_2 < z < 1. \tag{5.4}$$

By applying physical conditions, we determine the boundary conditions that must be satisfied at the ends $z = 0, 1$ of the tube as well as the matching conditions at the interfaces at $z = z_1, z_2$ between the flexible and rigid sections of the tube. At $z = z_1, z_2$, we must have continuity of pressure and continuity of axial volume flux. As the axial volume flux is proportional to $\tilde{w}$ and hence $\mathrm{d}\tilde{p}/\mathrm{d}z$, (see (4.6)) we have

$$[\tilde{p}]_-^+ = \left[\frac{\mathrm{d}\tilde{p}}{\mathrm{d}z}\right]_-^+ = 0, \quad \text{at} \quad z = z_1, z_2. \tag{5.5}$$

At the points where the elastic wall is clamped onto the rigid parts of the tube, we must have $\tilde{A} = 0$. Hence, using equation (4.7), we obtain the conditions

$$\frac{\mathrm{d}^2\tilde{p}}{\mathrm{d}z^2} = 0, \quad \text{at} \quad z = z_1, z_2. \tag{5.6}$$

In this model, we have fixed the total pressure at $z = 0$ as constant. As this constraint is a steady condition, any oscillations in pressure must have zero amplitude at the upstream end. Thus, we must have

$$\tilde{p} = 0 \quad \text{at} \quad z = 0. \tag{5.7}$$

Finally, the axial volume flux has been fixed at the downstream end. Because of this, the amplitude $\tilde{w}$ of the oscillatory axial velocity must be zero at $z = 1$. From (4.6), we find the final boundary condition

$$\frac{\mathrm{d}\tilde{p}}{\mathrm{d}z} = 0 \quad \text{at} \quad z = 1. \tag{5.8}$$

6. Solution for the Oscillatory Normal Modes

We now seek solutions of the governing equations (5.3) and (5.4) subject to the boundary and matching conditions (5.5)–(5.8). This is an eigenvalue problem for the oscillatory pressure $\tilde{p}(z)$ and the unknown frequency ω.

6.1 *Solution in the Rigid Sections of the Tube*

Solving (5.4) in the rigid sections of the tube ($0 < z < z_1$ and $z_2 < z < 1$) subject to the boundary conditions (5.7), (5.8), we find

$$\tilde{p} = Gz \quad \text{for} \quad 0 < z < z_1, \tag{6.1}$$

$$\tilde{p} = H, \quad \text{for} \quad z_2 < z < 1, \tag{6.2}$$

where G, H are some constants.

Combining the solutions (6.1) and (6.2) with the matching conditions (5.5), and eliminating the constant G between the resulting expressions at $z = z_1$, the following conditions on the solution in $z_1 < z < z_2$ are determined:

$$z_1 \frac{\mathrm{d}\tilde{p}}{\mathrm{d}z} - \tilde{p} = 0 \quad \text{at} \quad z = z_1, \tag{6.3}$$

$$\frac{\mathrm{d}\tilde{p}}{\mathrm{d}z} = 0 \quad \text{at} \quad z = z_2. \tag{6.4}$$

6.2 *General Solution in the Flexible Section of the Tube*

It is convenient to rewrite the system in terms of the scaled axial coordinate $\mathscr{Z}$ as introduced in (5.2). The governing ODE (5.3) is rewritten as

$$\frac{\mathrm{d}^4\tilde{p}}{\mathrm{d}\mathscr{Z}^4} + \frac{(M\omega^2 k_2 - k_0)(z_2 - z_1)^2}{k_2 \mathscr{F}} \frac{\mathrm{d}^2\tilde{p}}{\mathrm{d}\mathscr{Z}^2} - \frac{\omega^2 (z_2 - z_1)^4}{k_2 \mathscr{F}} \tilde{p} = 0. \tag{6.5}$$

The boundary conditions (5.6), (6.3) and (6.4) become

$$\frac{\mathrm{d}^2\tilde{p}}{\mathrm{d}\mathscr{Z}^2} = 0 \quad \text{at} \quad \mathscr{Z} = 0, 1, \tag{6.6}$$

$$\frac{z_1}{z_2 - z_1} \frac{\mathrm{d}\tilde{p}}{\mathrm{d}\mathscr{Z}} + \tilde{p} = 0 \quad \text{at} \quad \mathscr{Z} = 1, \tag{6.7}$$

$$\frac{\mathrm{d}\tilde{p}}{\mathrm{d}\mathscr{Z}} = 0 \quad \text{at} \quad \mathscr{Z} = 0. \tag{6.8}$$

Equation (6.5) is a fourth-order ODE with constant coefficients, and so has solutions of the form $\tilde{p} = e^{\lambda \mathscr{Z}}$. It may be shown (see Appendix B) that the eigenfrequencies ω are always real and non-zero. As the coefficient of $\tilde{p}$ in (6.5) is strictly negative, the quartic polynomial for λ always has one pair of real solutions and one pair of imaginary solutions. The general solution of (6.5) can be written as

$$\tilde{p}(\mathscr{Z}) = A\cosh g\mathscr{Z} + B\sinh g\mathscr{Z} + C\cos h\mathscr{Z} + D\sin h\mathscr{Z}, \tag{6.9}$$

where A, B, C and D are constants to be found, and $g > 0$ and $h > 0$ are defined by

$$g^2 = \frac{(z_2 - z_1)^2}{2k_2\mathscr{F}}\left[k_0 - M\omega^2 k_2 + \sqrt{(k_0 - M\omega^2 k_2)^2 + 4\omega^2 k_2\mathscr{F}}\right], \tag{6.10}$$

$$h^2 = \frac{(z_2 - z_1)^2}{2k_2\mathscr{F}}\left[M\omega^2 k_2 - k_0 + \sqrt{(k_0 - M\omega^2 k_2)^2 + 4\omega^2 k_2\mathscr{F}}\right]. \tag{6.11}$$

6.3 *Eigenfrequencies of the system*

Applying the boundary conditions (6.6)–(6.8) to the general solution (6.9) and eliminating the constants A, B, C and D, we find the following eigenvalue equation:

$$z_1\Big[2gh(1 - \cosh g\cos h) + (g^2 - h^2)\sinh g\sin h\Big] \\ -(z_2 - z_1)\frac{g^2 + h^2}{gh}\Big[g\sinh g\cos h + h\cosh g\sin h\Big] = 0. \tag{6.12}$$

The eigenvalue system (6.10)–(6.12) is conveniently solved by eliminating g and ω in order to obtain a single equation for h. First, we obtain an expression for ω in terms of g and h by considering the product of (6.10) and (6.11):

$$\omega^2 = \frac{g^2h^2k_2\mathscr{F}}{(z_2 - z_1)^4}. \tag{6.13}$$

Taking the difference between (6.10) and (6.11), and using (6.13) to eliminate ω, we obtain

$$g = \left[\frac{\frac{k_0(z_2-z_1)^2}{k_2\mathscr{F}} + h^2}{1 + \frac{Mh^2k_2}{(z_2-z_1)^2}}\right]^{\frac{1}{2}}. \tag{6.14}$$

We now use (6.14) to eliminate g from (6.12), giving us an equation to be solved for a single unknown h. Solving numerically using Maple, we find countably many solutions for h. The relationship (6.14) is then used to recover g and finally (6.13) is used to find the eigenfrequencies ω. We denote the nth eigenfrequency as ω_n, with ω_1 being the fundamental mode.

We observe that as $\omega \to \infty$, $g = O(1)$ and $h = O(\omega)$. Hence, for large ω the eigenvalue equation (6.12) is approximately

$$-z_1h^2\sinh(g)\sin(h) - \frac{(z_2 - z_1)h^2}{g}\cosh(g)\sin(h) = 0. \tag{6.15}$$

Hence we expect to find solutions at $h \simeq n\pi$, for large integers n. This approximation is helpful when computing the numerical solutions.

7. Stability Criterion and Growth Rate

The leading-order solution found above comprises normal modes that are all predicted to be neutrally stable. At higher orders these modes will be expected to slowly grow or decay. We now follow Whittaker *et al.* (**31**), who showed that it is possible to derive these growth rates by considering the global energy budget of the system. By subtracting off the mean-flow components, this energy budget can be expressed as

$$\frac{\mathrm{d}}{\mathrm{d}t}\left(\tilde{\mathbb{E}}_s + \tilde{\mathbb{E}}_f\right) = \frac{1}{\ell St}\left(\mathscr{K} - \mathscr{S} - \mathscr{D}\right). \tag{7.1}$$

Here, $\tilde{\mathbb{E}}_s$ is the total dimensionless energy due to oscillations in the tube wall and $\tilde{\mathbb{E}}_f$ is the dimensionless oscillatory kinetic energy in the fluid, both averaged over a period of the oscillations. On the right-hand side we have three energy fluxes associated with the oscillatory component of the flow: $\mathscr{K}$ is the mean flux of kinetic energy through the ends of the tube due to the oscillatory perturbation, $\mathscr{S}$ is the mean rate of working by oscillatory pressure forces that arise at the tube ends, and $\mathscr{D}$ is the mean rate of dissipation in the oscillatory viscous Stokes layer adjacent to the tube wall. The energies and fluxes have been non-dimensionalized using the scalings (2.17).

By substituting expressions for $\tilde{\mathbb{E}}_s$, $\tilde{\mathbb{E}}_f$, $\mathscr{K}$, $\mathscr{S}$ and $\mathscr{D}$ — calculated from the leading-order normal-mode solutions in §6 — into (7.1), we are able to derive an equation for the evolution of the amplitude $\Delta(t)$.

7.1 *Energy Fluxes, Fluid Energy and Wall Energy*

Whittaker *et al.* (**27**, **31**) showed that $\mathscr{K}$, $\mathscr{S}$, $\mathscr{D}$ and $\tilde{\mathbb{E}}_f$ are given by

$$\mathscr{K} = \frac{3}{4}\pi\ell^2 St^2\Delta^2|\tilde{w}(0)|^2, \tag{7.2}$$

$$\mathscr{S} = \frac{1}{4}\pi\ell^2 St^2\Delta^2|\tilde{w}(0)|^2, \tag{7.3}$$

$$\mathscr{D} = \frac{\pi\ell^3 St^3\Delta^2(2\omega)^{\frac{1}{2}}}{2\alpha}\int_0^1 |\tilde{w}(z)|^2\mathrm{d}z, \tag{7.4}$$

$$\tilde{\mathbb{E}}_f = \frac{\Delta^2 St^2 A_0\ell^2}{4}\int_0^1 |\tilde{w}(z)|^2\mathrm{d}z. \tag{7.5}$$

These expressions concern energies and fluxes in the fluid, and are evaluated purely from the leading-order axial oscillatory fluid flow $\tilde{w}(z)$. Hence the expressions are unchanged by the addition of wall inertia.

However, a new expression for the energy $\tilde{\mathbb{E}}_s$ in the wall must be derived here, taking into account not only the elastic energy also but the kinetic energy too. This calculation is detailed in Appendix C, where it is shown that

$$\tilde{\mathbb{E}}_s = \frac{\Delta^2 St^2 A_0\ell^2}{4\omega^2}\int_0^1 \left|\tilde{p}'(z)\right|^2 + 2k_2M\left|\tilde{p}''(z)\right|^2\,\mathrm{d}z. \tag{7.6}$$

We note that in the absence of wall inertia ($M = 0$), (7.6) matches the expression for $\tilde{\mathbb{E}}_s$ derived in (**27**, **31**).

7.2 *Growth Rate*

Now we have expressions for the various energies and fluxes, we can use these along with (7.1) to find an expression for the growth rate of each of the normal modes and thence a stability criterion. From the expressions (7.5) for $\tilde{\mathbb{E}}_f$ and (7.6) for $\tilde{\mathbb{E}}_s$, and using (4.6) to express $\tilde{w}$ in terms of $\tilde{p}$, we see that

$$\tilde{\mathbb{E}}_s + \tilde{\mathbb{E}}_f = \frac{\Delta^2 St^2 A_0 \ell^2}{2\omega^2} \int_0^1 |\tilde{p}'(z)|^2 + k_2 M |\tilde{p}''(z)|^2 \mathrm{d}z. \tag{7.7}$$

From the expressions (7.2)–(7.4) for $\mathscr{K}$, $\mathscr{S}$ and $\mathscr{D}$, and using (4.6) to express $\tilde{w}$ in terms of $\tilde{p}$, we have

$$\mathscr{K} - \mathscr{S} - \mathscr{D} = \frac{\Delta^2 St^2 \ell^2 \pi}{2\omega^2} \left[|\tilde{p}'(0)|^2 - \frac{\ell St (2\omega)^{\frac{1}{2}}}{\alpha} \int_0^1 |\tilde{p}'(z)|^2 \mathrm{d}z \right]. \tag{7.8}$$

Substituting (7.7)–(7.8) into (7.1) and evaluating the time derivative on the left-hand side, we obtain

$$\frac{\mathrm{d}\Delta}{\mathrm{d}t} = \left[\frac{\pi}{2A_0} \left(\frac{\frac{|\tilde{p}'(0)|^2}{\ell St} - \frac{(2\omega)^{\frac{1}{2}}}{\alpha} \int_0^1 |\tilde{p}'(z)|^2 \mathrm{d}z}{\int_0^1 |\tilde{p}'(z)|^2 + k_2 M |\tilde{p}''(z)|^2 \mathrm{d}z} \right) \right] \Delta. \tag{7.9}$$

Hence, the amplitude of each normal mode $\tilde{p}(z)$ grows or decays exponentially and we may write

$$\Delta(t) = \Delta_0 e^{\Lambda t}, \tag{7.10}$$

where Δ_0 is the initial amplitude of the oscillations, and the growth rate Λ is given by

$$\Lambda = \frac{\pi}{2A_0} \left(\frac{\frac{|\tilde{p}'(0)|^2}{\ell St} - \frac{(2\omega)^{\frac{1}{2}}}{\alpha} \int_0^1 |\tilde{p}'(z)|^2 \mathrm{d}z}{\int_0^1 |\tilde{p}'(z)|^2 + k_2 M |\tilde{p}''(z)|^2 \mathrm{d}z} \right). \tag{7.11}$$

7.3 *Stability Criterion*

When $\Lambda = 0$, neutrally stable oscillations are obtained. We define the critical Reynolds number Re_c to be the Reynolds number (defined by $Re = \alpha^2/St$) at which $\Lambda = 0$. (If the other parameters are held constant, then Re is a measure of the mean flow rate through the tube.) Using the expression (7.11) for the growth rate, we find

$$Re_c = \frac{\alpha \ell (2\omega)^{\frac{1}{2}}}{|\tilde{p}'(0)|^2} \int_0^1 |\tilde{p}'(z)|^2 \mathrm{d}z. \tag{7.12}$$

Using this expression for Re_c, the growth rate Λ may be written as

$$\Lambda = \frac{\pi (Re - Re_c) |\tilde{p}'(0)|^2}{2A_0 \ell \alpha^2 \int_0^1 |\tilde{p}'(z)|^2 + k_2 M |\tilde{p}''(z)|^2 \mathrm{d}z}. \tag{7.13}$$

$\mathscr{F}$	M	ω_1	ω_2	ω_3	ω_4	ω_5
0.01	0	6.108	19.06	33.80	50.86	70.67
0.01	0.001	6.091	18.60	31.61	44.81	57.98
0.01	0.01	5.948	15.55	21.62	25.74	29.14
0.01	0.1	4.912	7.728	8.563	9.274	10.03
0.01	1	2.389	2.639	2.792	2.985	3.210
0.1	0	6.991	25.73	54.31	94.37	146.5
0.1	0.001	6.970	25.08	50.68	82.96	120.0
0.1	0.01	6.795	20.82	34.41	47.54	60.37
0.1	0.1	5.545	10.24	13.64	17.23	20.87
0.1	1	2.638	3.514	4.481	5.565	6.694
1	0	11.80	59.41	144.3	268.1	431.4
1	0.001	11.76	57.88	134.6	235.6	353.3
1	0.01	11.45	47.96	91.30	135.1	177.8
1	0.1	9.259	23.63	36.29	49.08	61.51
1	1	4.360	8.148	11.96	15.86	19.75

Table 1 Asymptotic predictions for the eigenfrequencies ω_n of the normal modes, for different values of the axial tension parameter $\mathscr{F}$ and the wall inertia parameter M, when $z_1 = 0.1$, $z_2 = 0.9$ and $\sigma_0 = 0.6$.

The growth rate Λ and critical Reynolds number Re_c depend both on the problem parameters and the particular mode being considered. When $Re \leq Re_c$ for every mode, the system will be stable. If $Re > Re_c$ for any mode, then the system will be unstable to that oscillatory mode of perturbation. Wall inertia affects Λ and Re_c both explicitly through the parameter M, and also implicitly through the mode shapes $\tilde{p}$ and frequencies ω.

8. Asymptotic Predictions

8.1 *The Effect of Wall Inertia on the Frequencies ω*

The numerical approach outlined in §6.3 is used to determine the eigenfrequencies ω_n of the model for different values of the axial tension parameter $\mathscr{F}$ and wall inertia parameter M. The tube geometry is kept fixed, with $z_1 = 0.1$, $z_2 = 0.9$ and $\sigma_0 = 0.6$ as in (**31**). (Using this value for σ_0, we have $k_0 = 11.07487$, $k_2 = 1.70441$ and $A_0 = 2.73060$.) The results are shown in table 1.

It is seen from the table that the addition of wall inertia significantly reduces the values of the eigenfrequencies ω_n for the higher-order modes, even when M is small. However for the fundamental modes, the effect of wall inertia is only significant when M is larger than around 0.1. Finally, it is noted that for larger values of M, the eigenfrequencies increase much more slowly as the mode number n is increased.

8.2 *The Effect of Wall Inertia on $\tilde{p}$, $\tilde{w}$ and $\tilde{A}$*

Using the values of the eigenfrequencies ω_n, we determine the corresponding normal modes of the pressure $\tilde{p}_n$, the axial velocity $\tilde{w}_n$ and the area $\tilde{A}_n$. We obtain $\tilde{p}_n$ by applying the

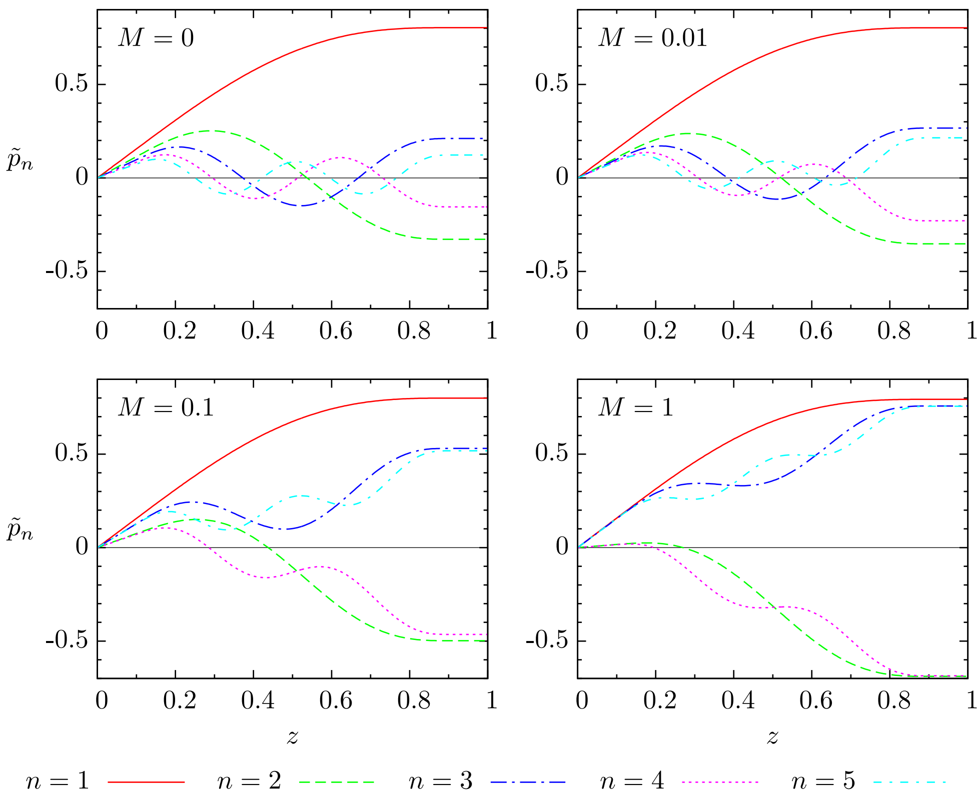

Fig. 3 Asymptotic predictions for the first five normal modes of $\tilde{p}_n$, for different values of M, when $\mathscr{F}=1$, $z_1=0.1$, $z_2=0.9$ and $\sigma_0=0.6$. The solutions have been normalised such that $\int_0^1 |\tilde{p}_n'|^2 dz = 1$ and $\tilde{p}_n'(0) > 0$.

boundary conditions (6.6)–(6.8) to (6.9)–(6.11). We choose the normalisation

$$\int_0^1 |\tilde{p}_n'|^2 \mathrm{d}z = 1, \qquad \tilde{p}_n'(0) > 0, \tag{8.1}$$

motivated by the form of Re_c in (7.12). Then (4.6) and (4.7) allow us to find the corresponding $\tilde{w}_n$ and $\tilde{A}_n$.

In Fig. 3, we show the first five normal modes of $\tilde{p}_n$, plotted for different values of M. From the figure, we see little observable change in the fundamental mode for any of the values of M. However for higher-order modes, there are notable changes as M increases. For $M \gtrsim 0.1$, rather than being dominated by oscillations in z about $\tilde{p}_n = 0$, the eigenfunctions $\tilde{p}_n$ also have a significant linear component in z.

Fig. 4 shows $\mathrm{i}\tilde{w}_n$ for the first five normal modes. Again there is very little difference between the modes for $M = 0, 0.01$. However, in the cases where $M = 0.1$ and $M = 1$, the higher-order modes oscillate in z about a non-zero value of $\mathrm{i}\tilde{w}_n$.

Finally, Fig. 5 shows the first five normal modes of $\tilde{A}_n$. As before, it is seen that there is

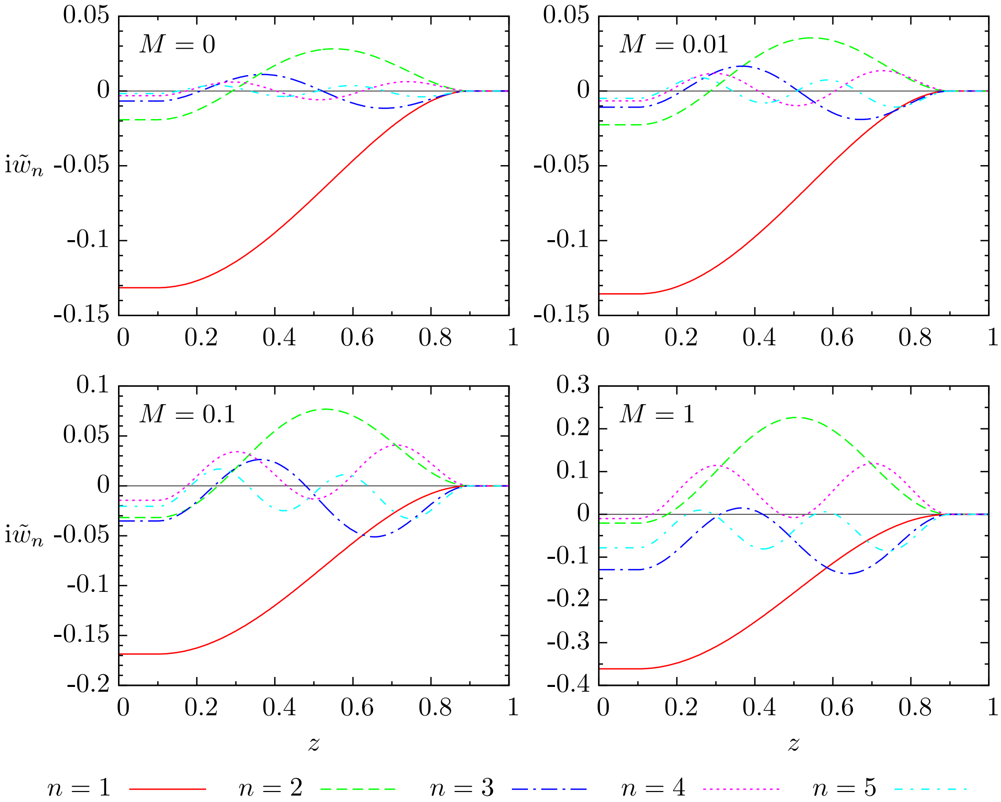

Fig. 4 Asymptotic predictions for the first five normal modes of $\mathrm{i}\tilde{w}_n$, for different values of M when $\mathscr{F} = 1$, $z_1 = 0.1$, $z_2 = 0.9$ and $\sigma_0 = 0.6$. The normalisation is as in Fig. 3. (Note the different vertical scales used on the two lower plots.)

not much difference between the modes when $M = 0$ and $M = 0.01$. However, in the cases $M = 0.1$ and $M = 1$, it can be seen that the fundamental mode $\tilde{A}_1$ tends towards being symmetric about $z = 0.5$. It is also noted that unlike the modes for the pressure $\tilde{p}_n$ and axial velocity $\tilde{w}_n$, the higher-order modes for the area oscillate in z about $\tilde{A}_n = 0$, for all values of M.

8.3 *The Effect of Wall Inertia on Re_c and Λ*

The critical Reynolds number Re_c and growth rate Λ are found from the normal-mode solutions using (7.12) and (7.13). In Fig. 6, we plot Re_c against M for the first four eigenmodes. From the plots, we see there are significant differences in the behaviour of the modes with odd and even n as M increases. For the odd modes, Re_c decreases as M increases, while for even modes Re_c increases as M increases. Thus the odd modes are destabilised by adding wall inertia, while the even modes are stabilised. We also see that, at least for $0 \leq M \leq 1$ the mode with the smallest Re_c and therefore the most unstable, is still the fundamental $n = 1$ mode.

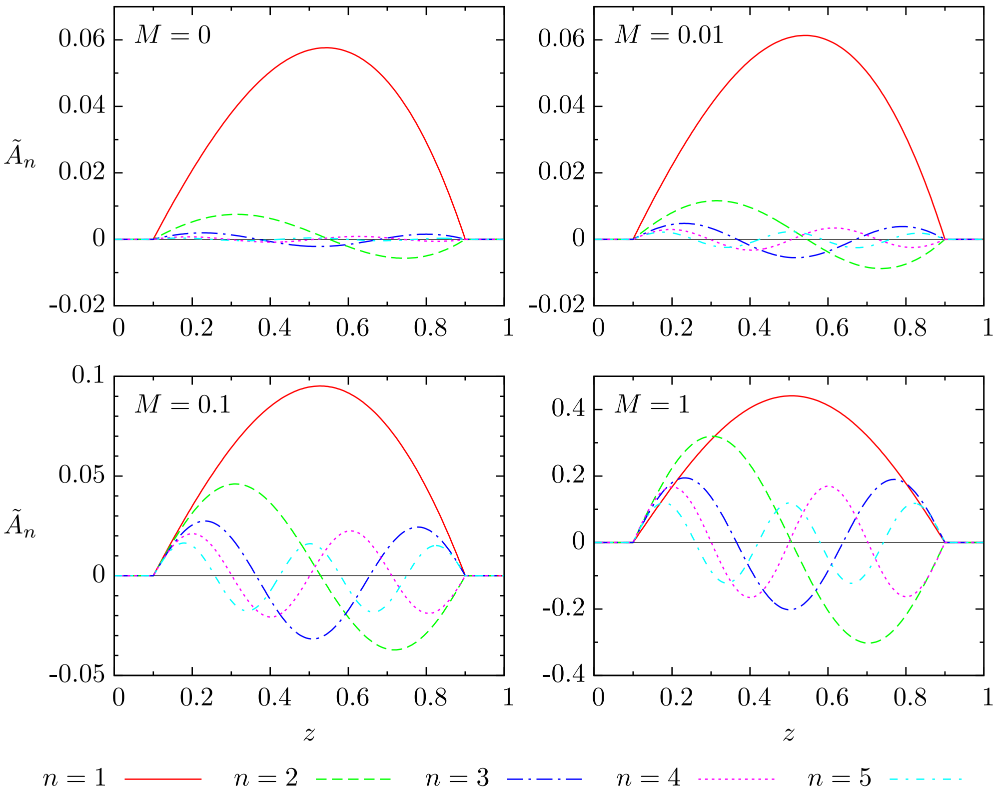

Fig. 5 Asymptotic predictions for the first five normal modes of $\tilde{A}_n$, for different values of M when $\mathscr{F} = 1$, $z_1 = 0.1$, $z_2 = 0.9$ and $\sigma_0 = 0.6$. The normalisation is as in Fig. 3. (Note the different vertical scales used on the two lower plots.)

In Fig. 7, we show plots of $\partial\Lambda/\partial Re$, which captures the sensitivity in the growth rate to changes in the mean flow along the tube. For all four modes, as M increases, the gradient of Λ for a given A_0, α and ℓ tends to zero. So wall inertia acts as a damping effect, decreasing the sensitivity of the system. However this damping is seen to be much more significant for even modes than for odd modes.

9. Comparison with Direct Numerical Simulations

9.1 *Method for Numerical Solution*

To evaluate the accuracy of our asymptotic predictions, we conducted numerical simulations of the onset of self-excited oscillations in elliptical collapsible tubes. In these simulations, the three dimensional unsteady Navier–Stokes equations, coupled to the equations of large-displacement Kirchhoff–Love shell theory, were discretized using the object-oriented multi-physics finite-element library `oomph-lib` (**36**). The implementation and validation of these simulations is detailed by Heil and Boyle (**37**) in their study of the onset of self-excited oscillations in initially circular cylindrical tubes.

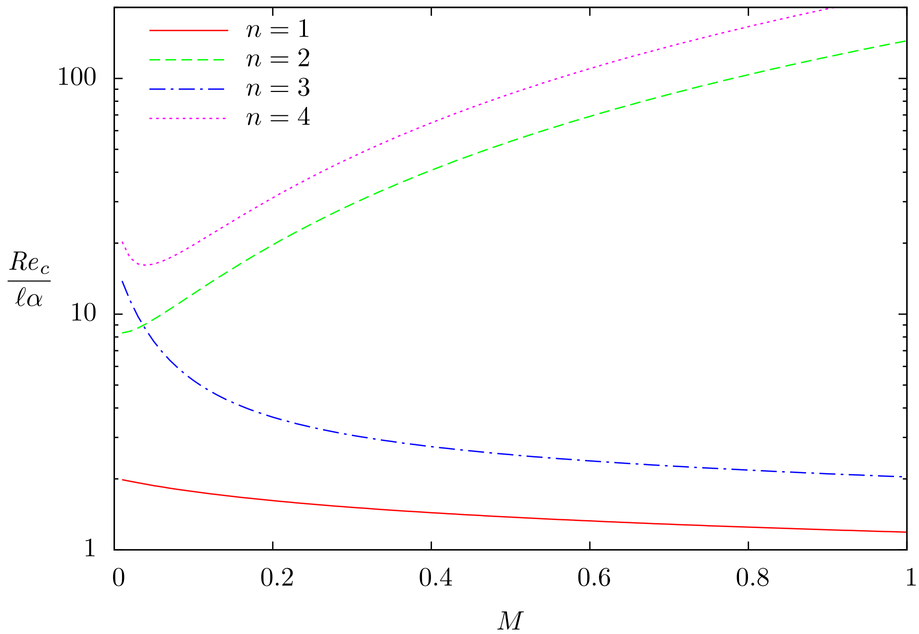

Fig. 6 Asymptotic predictions for the the critical Reynolds number Re_c as a function of M from (7.12), with $z_1 = 0.1$, $z_2 = 0.9$, and $\sigma_0 = 0.6$, for mode numbers $n \in \{1, 2, 3, 4\}$. Note the differing behaviour of the odd and even modes as M increases.

In the numerical simulations performed here, the cross sections of the undeformed tube were set to be elliptical, and parallel inflow and outflow was imposed at the upstream and downstream ends of the system. Additionally, the flow rate at the downstream end was controlled, the fluid at the upstream end was subject to zero axial traction (corresponding to setting zero fluid pressure), and the steady external pressure $\bar{p}_{\text{ext}}$ was set to $\bar{p}_{\text{ext}} = -\bar{G}/2$, where $\bar{G}$ is defined by (4.4). As such, $\bar{p}_{\text{ext}}$ is equal to the fluid pressure at the midpoint of the elastic-walled tube with steady Poiseuille flow in the undeformed state.

Each simulation was started with an initial condition where the tube wall is in its undeformed configuration with the velocity field within the tube being given by steady Poiseuille flow for this configuration. In order to initiate small-amplitude oscillations, $\bar{p}_{\text{ext}}$ was increased by a small amount so that the tube wall started to collapse slightly at the beginning of the simulation. When the displacement of a control point situated on the tube's minor half axis halfway along the tube exceeded 0.5% of its initial radius, $\bar{p}_{\text{ext}}$ was then re-set to $-\bar{G}/2$. Once any transients had decayed, the system performed small-amplitude oscillations about the steady configuration, and the period and growth or decay rates of these oscillations were extracted by fitting the time trace of the displacements to an exponentially growing or decaying harmonic oscillation. The standard resolution for the simulations presented here involved 48,398 degrees of freedom. Selected simulations were

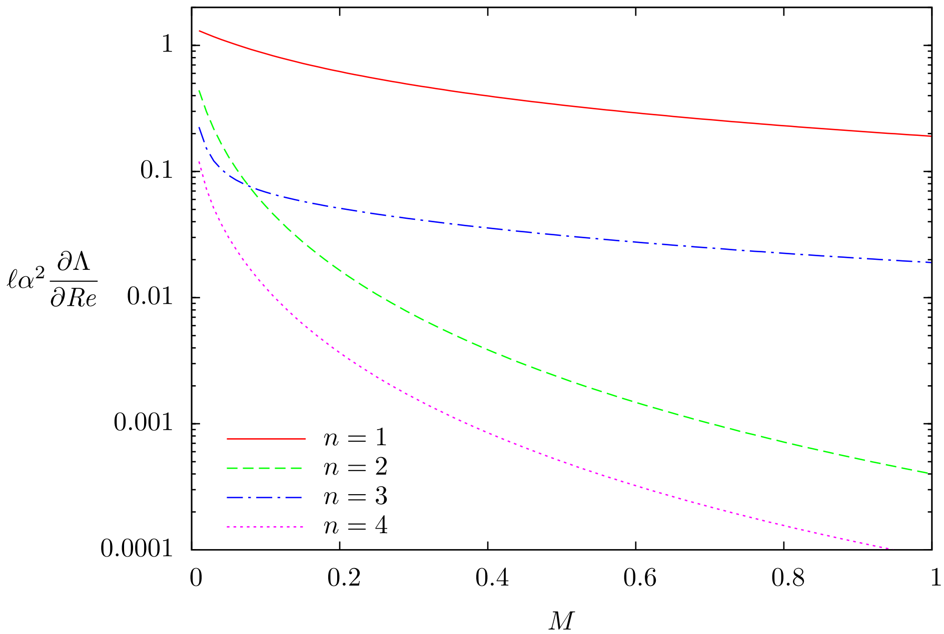

Fig. 7 Asymptotic predictions for the gradient $\partial\Lambda/\partial Re$ of the growth rate as a function of M, with $z_1 = 0.1$, $z_2 = 0.9$, $\sigma_0 = 0.6$, for mode numbers $n \in \{1, 2, 3, 4\}$ This demonstrates the sensitivity of the growth rate to the mean-flow Reynolds number. Again note the differing behaviour of the odd and even modes and M increases.

repeated with an increased spatial resolution with 75,136 degrees of freedom to verify the mesh-independence of the results.

9.2 *Comparison of Numerical Results and Asymptotic Predictions*

We compare the asymptotic predictions and the numerical results for

$$\sigma_0 = 0.6, \quad z_1 = 0.1, \quad z_2 = 0.9, \quad \mathscr{F} = 1, \quad \ell = 15, \quad \alpha^2 = 50, \tag{9.1}$$

where $\sigma_0 = 0.6$ also implies

$$A_0 = 2.73060, \quad k_0 = 11.07487, \quad k_2 = 1.70441. \tag{9.2}$$

The remaining parameters, St (or equivalently Re) and M are varied between the different simulations.

In Fig. 8, we plot the analytical approximations and numerical calculations for the eigenfrequency ω_1 of the fundamental mode, first against Re for different values of M in Fig. 8(a), and then against M in Fig. 8(b). It is seen in Fig. 8(a) that as in the asymptotic predictions, the numerical results indicate that varying the Reynolds number Re gives negligible change in ω_1. In both plots, there is excellent agreement between the asymptotic predictions and the numerical simulations.

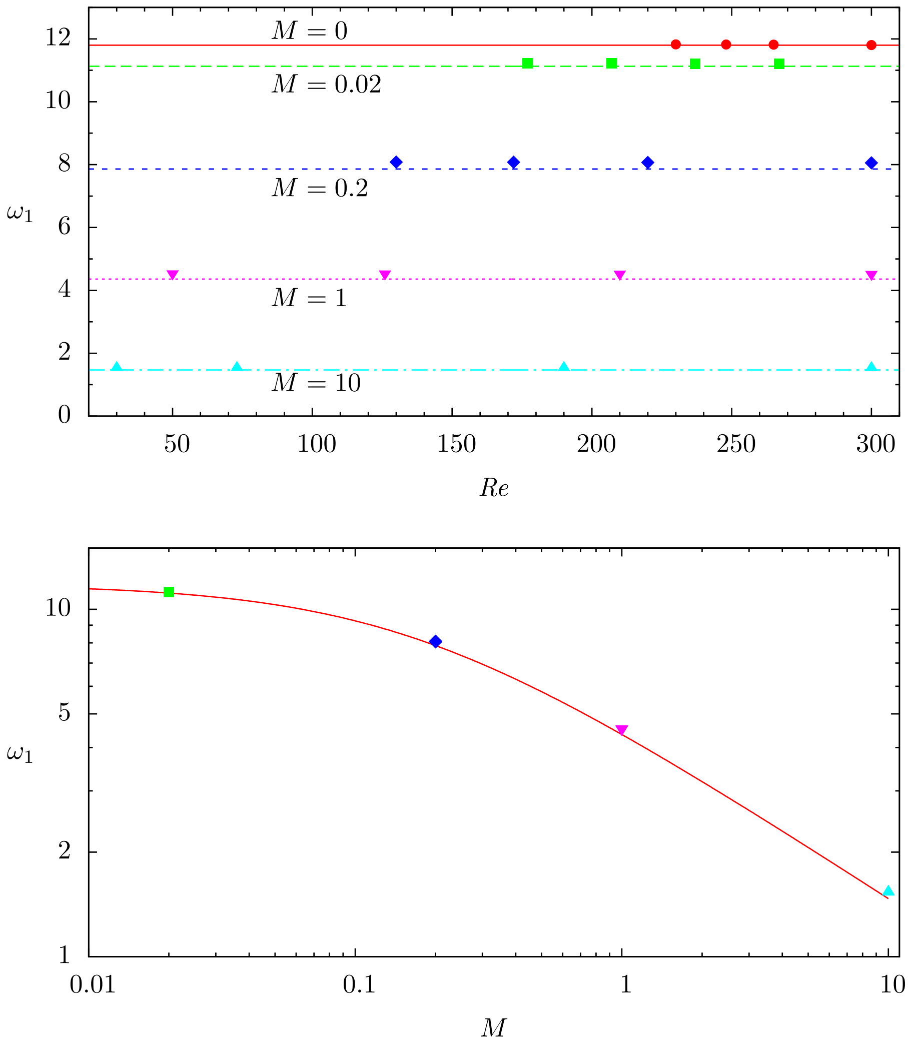

Fig. 8 Comparison of the asymptotic predictions and the numerical results for the eigenfrequency ω_1 of the fundamental mode for $\sigma_0 = 0.6$, $z_1 = 0.1$, $z_2 = 0.9$, $\mathscr{F} = 1$, $\ell = 15$, $\alpha^2 = 50$. In (a), the asymptotic predictions (solid lines) and numerical results (points) for ω_1 are plotted against Re for $M = 0, 0.02, 0.2, 1, 10$ in red, blue, green, black and brown respectively. In (b), the asymptotic predictions (solid line) and the numerical results (points) seen in (a) for ω_1 are plotted against M. Note that the numerical results for different values of Re and the same M are indistinguishable on this scale.

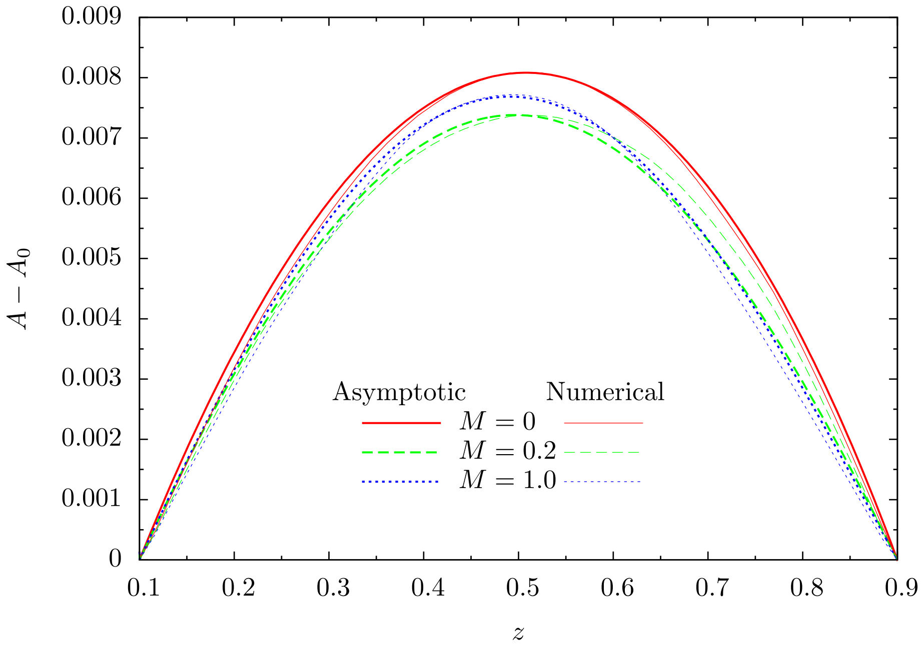

Fig. 9 Comparison of theoretical approximations and numerical calculations for the total area variation $A - A_0$ along the length of the tube, for $\sigma_0 = 0.6$, $z_1 = 0.1$, $z_2 = 0.9$, $\mathscr{F} = 1$, $\ell = 15$, $\alpha^2 = 50$ and $M \in \{0, 0.2, 1\}$. The numerical results (thinner lines) have been calculated for $Re = 248$, $t = 1.564$ when $M = 0$, $Re = 172$, $t = 3.063$ when $M = 0.2$, and $Re = 126$, $t = 5.449$ when $M = 1$. The values of Re are chosen to be near the critical Reynolds number Re_{c1} for the fundamental mode so the amplitude of this mode has only slow variation in time, and the values of t are chosen to be near the times where the area variation is maximal. The theoretical approximations (thicker lines) of $A - A_0$ are calculated using the expression (2.16) for A, the expression (5.1) for $\bar{A}$, and the normalised fundamental mode $\tilde{A}_1$ for the oscillatory component of the area variation, as seen in Fig. 5. The value of the amplitude Δ of the oscillatory component is set to be $\Delta = 0.114, 0.0443, 0.0138$ when $M = 0, 0.2, 1$ respectively, in order to match the amplitude of the area variation between the theoretical approximations and numerical results.

In Fig. 9, we compare the asymptotic predictions and numerical results for the variation in $A - A_0$ along the length of the tube in the cases $M = 0, 0.2, 1$. Here, the numerical simulations are plotted using Reynolds numbers close to the analytically predicted values of the critical Reynolds number Re_{c1} of the fundamental mode, so that the growth rate of this mode is small and the amplitude of this mode has little variation throughout the simulation. The values of time t were set so that the numerical results for $A - A_0$ are near their maxima. To obtain an asymptotic prediction for $A - A_0$, we used the expression (2.16) for A and the expression (5.1) for $\bar{A}$, along with the normalised fundamental mode $\tilde{A}_1$ for the oscillatory component of the area variation as seen in Fig. 5. The amplitude Δ of the oscillatory component was set so that the amplitude of the area variation matches between the asymptotic prediction and numerical results. From the figure, it is seen that

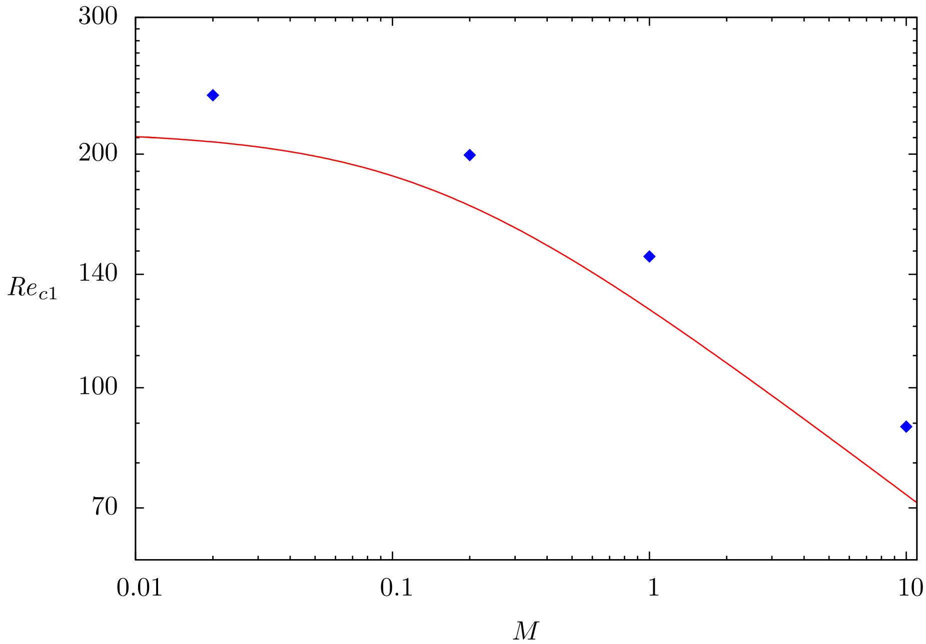

Fig. 10 Comparison of the theoretical approximation (7.12) and numerical calculations for the critical Reynolds number Re_{c1} of the fundamental mode against M, for $\sigma_0 = 0.6$, $z_1 = 0.1$, $z_2 = 0.9$, $\mathscr{F} = 1$, $\ell = 15$, $\alpha^2 = 50$. The asymptotic prediction is given by the solid line, and the numerical calculations are given by the points.

as in the asymptotic predictions, the peaks of $A - A_0$ in the numerical simulations move slightly towards the upstream end of the tube as M is increased. We also also observe that there is good agreement between the asymptotic predictions and numerical results for all values of M.

The asymptotic prediction (7.12) and numerical calculations for the critical Reynolds number Re_{c1} of the fundamental mode are shown in Fig. 10 as functions of M. From the figure, we see that the asymptotic prediction captures the qualitative behaviour well but systematically underestimates the value of Re_{c1} by about 13–18%.

Finally, in Fig. 11, the asymptotic prediction (7.13) and numerical results for the growth rate Λ_1 of the fundamental and fastest growing mode are plotted against Re for the cases $M = 0, 0.2, 1, 10$. From the figure, we see that both the theoretical and numerical results vary linearly with the Reynolds number, with the same gradient for each value of M. Furthermore, although the theoretical results systematically overestimate the value of Λ_1, this error decreases with increasing M to the point where the theoretical and numerical results are almost indistinguishable in the case of $M = 10$.

Overall, the asymptotic predictions derived in this paper are in good agreement the numerical simulations for the frequency ω_1 and area variation $A - A_0$ of the fundamental mode. Although the asymptotic predictions underestimate the value of the critical Reynolds

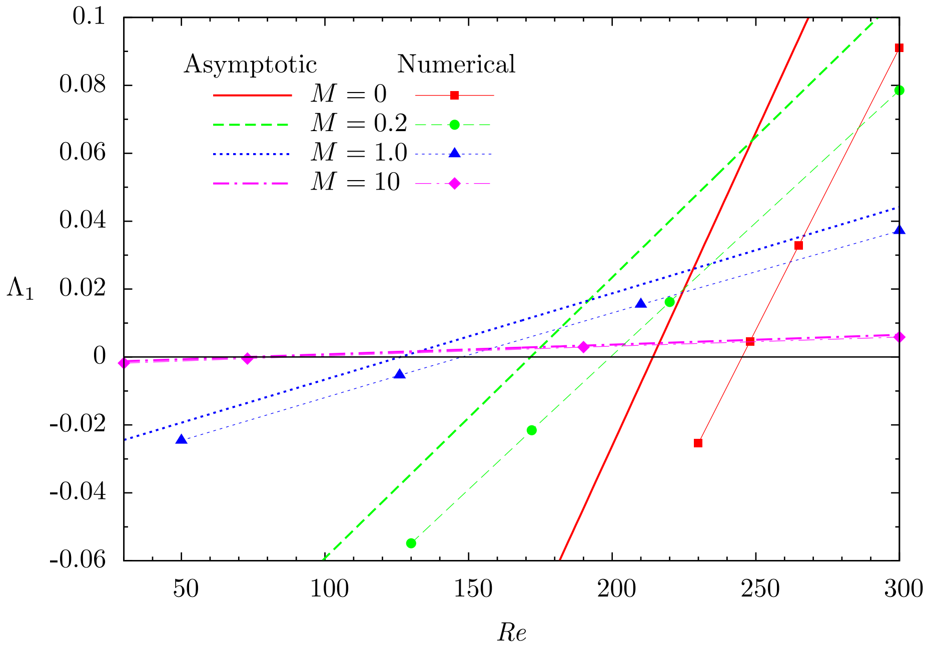

Fig. 11 Comparison of the theoretical approximation (7.13) and numerical calculations for the growth rate Λ_1 of the fundamental mode against Re, for $\sigma_0 = 0.6$, $z_1 = 0.1$, $z_2 = 0.9$, $\mathscr{F} = 1$, $\ell = 15$, $\alpha^2 = 50$, and $M \in \{0, 0.2, 1, 10\}$. The asymptotic predictions are given by the thicker lines, whereas the numerical results are given by the points joined by the thinner lines.

number Re_{c1}, and overestimate the value of the growth rate Λ_1 of the fundamental mode, they still capture the qualitative behaviour of these quantities. The error in the approximation for Λ_1 decreases with increasing wall inertia. Given the number of approximations made in order to obtain the asymptotic predictions, and the fact that the various 'small' parameters are not all that small in the cases considered here, we believe that the discrepancies observed are acceptable, and are confident that the asymptotic system is indeed capturing the essential physics of the full problem.

10. Discussion and Conclusions

In this paper, we have studied the effects of wall inertia on the onset of high-frequency long-wavelength self-excited oscillations in flow through an elastic-walled tube. The previous model of Whittaker *et al.* (**31**) has been extended to include inertial resistance to the motion of the elastic wall. The effect of wall inertia in the new model is characterised by a single parameter M, which is defined in (2.9) as the ratio of the inertial to azimuthal bending resistance in the wall. We have quantified the effects of M on the modes of oscillation and their stability.

Asymptotic analysis, based on the limit of high-frequency long wavelength small-amplitude oscillations in a thin-walled tube, allowed us to reduce the system to a one-dimensional eigenvalue problem (6.5)–(6.8) for the leading-order pressure perturbation amplitude $\tilde{p}(z)$. The eigenvalue equation (6.12) was solved numerically to determine the frequencies ω, and a countable set of neutrally stable oscillatory normal modes were found. The global energy budget was used to derive the slow growth or decay rates Λ of each of these modes (a first-order effect, but completely determined by the leading-order solution). As in (**31**), a critical point was found for each mode to be neutrally stable. This was expressed as a critical mean-flow Reynolds number Re_c, with the system being stable for lower Reynolds numbers and unstable for higher Reynolds numbers. The asymptotic expressions for the critical Reynolds number Re_c and the growth rate Λ were found in (7.12) and (7.13). The fundamental mode with the smallest number of axial oscillations was found to have the lowest-frequency and the highest growth rate. The critical Reynolds number for this mode therefore gave the stability boundary for the system.

It is interesting to note that wall inertia does not enter the governing equation (6.5) in the same way that the fluid inertia does. (Compare the $M\omega^2$ term associated with wall inertia to the ω^2 one associated with fluid inertia.) The effect on the fluid pressure from the wall inertia is directly proportional to the area changes $\tilde{A}$ at each z. However, the effect on the fluid pressure from the fluid inertia is a result of two axial integrals of $\tilde{A}$ (one to obtain the axial fluid velocity using (4.5), and one to integrate the pressure gradient using (4.6)).

Full numerical simulations have also been conducted, for a number of different parameter sets, using the object-oriented multi-physics finite-element library `oomph-lib`. Our asymptotic predictions compare reasonably well with these numerical simulations when the small parameters in the asymptotics are of size $O(0.1)$. The normal modes and frequencies show excellent agreement (Fig. 8 and Fig. 9). The growth rates and critical Reynolds numbers agree less well (Fig. 10 and Fig. 11), but the qualitative behaviour is captured and the discrepancies are still within acceptable bounds.

In both the numerical simulations and the asymptotic predictions, wall inertia (through the parameter M) can be seen to affect the modes and the stability results in three distinct ways. First it alters the mode shapes $\tilde{p}(z)$ through the M in the governing equation (6.5). As M increases, the complementary function for (6.5) approaches a linear combination of harmonic and linear functions of z. This increases the symmetry of the modes, as seen in figures 3–5. (Physically, the oscillations are governed more by a local balance between wall inertia and axial tension effects, with the symmetry-breaking fluid inertia becoming less important.) As a result of the increased symmetry, the axial sloshing flows increasingly cancel out between adjacent peaks and troughs in the wall displacements $\tilde{A}$. For even modes, these cancellations significantly reduce the sloshing flow at the upstream end, and thus weaken the instability. For odd modes, the unmatched peak still gives a sloshing flow at the upstream end, although the magnitude is decreased slightly. The effect enters the expression (7.12) for the critical Reynolds number Re_c through the $\tilde{p}'(0)$ factor, where a lower value of $\tilde{p}'(0)$ causes a higher Re_c, thus giving a more stable mode. As can be seen in Fig. 3, $\tilde{p}'(0)$ is significantly reduced for even modes, and hence this is a significant stabilising effect. However, for the fundamental mode (which is odd), this effect only represents a small stabilising effect.

Secondly, M affects the frequency of the normal modes. As would be expected, the addition of extra inertia reduces the frequency of the normal-mode oscillations. The effect of this in (7.12) is to reduce the critical Reynolds number Re_c, thus destabilising the modes.

Physically, this effect arises as follows. In (7.2)–(7.4) the kinetic energy flux $\mathscr{K}$ and rate of working flux $\mathscr{S}$ both contain the same power of ω, but the viscous dissipation $\mathscr{D}$ has an additional factor of $\omega^{1/2}$. (The viscous Stokes layers are $O(\omega^{1/2})$ thick, and have $O(\omega^{-1/2})$ velocity gradients. The velocity-gradient-squared integrated over the thickness gives the $\omega^{1/2}$ factor.) Hence reducing the frequency reduces the dissipative losses relative to the other energy fluxes, thus destabilising the mode.

Finally, M affects the oscillatory energy contained in each normal mode. This is because the inclusion of inertia in the wall implies the presence of kinetic energy in the wall. This appears as the M term in the expression (7.6) for the mean oscillatory energy $\tilde{\mathbb{E}}_s$ in the wall. (The other term in (7.6) corresponds to the mean elastic potential energy from bending and stretching.) As M increases, the energy in the wall for oscillations of a given shape, frequency and amplitude increases. This means that for the amplitude of the mode to increase or decrease by a given amount, more energy must be gained or lost from the system. If the energy fluxes remain fixed then the growth and decay rates of each mode will be damped, i.e. $|\Lambda|$ decreases. In the expression (7.13) for the Λ, this takes effect through the M in integral in the denominator.

Overall, an increase in wall inertia is a destabilising effect, in that it reduces the critical mean-flow Reynolds number for the fundamental mode. This effect is brought about primarily through the lowering of the frequency of the mode, and the resultant decrease in dissipative losses. However, the increase in energy in the oscillations caused by the kinetic energy of the wall means that the growth rates are damped by increasing amounts as more wall inertia is added. At higher Reynolds numbers this effect dominates, and the growth rates are reduced by an increase in wall inertia. In this regime wall inertia acts as a stabilising effect.

Acknowledgements

MCW gratefully acknowledges support from the University of East Anglia in the form of a funded PhD Studentship.

References

1. D. A. McDonald, *Blood flow in arteries*. Edward Arnold, 2nd edn. (1974).

2. J. Lighthill, *Mathematical Biofluiddynamics*. Soc. Ind. Appl. Math. (1975).

3. T. J. Pedley, *The Fluid Mechanics of Large Blood Vessels*. Camb. Univ. Press (1980).

4. M. Heil and O. E. Jensen, Flows in deformable tubes and channels: theoretical models and biological applications. In P. W. Carpenter and T. J. Pedley, editors, *Flow past highly compliant boundaries and in collapsible tubes*, chap. 2, pages 15–49, Springer (2003).

5. S. Rodbard and L. Takacs, Hydrodynamics of autoregulation. *Cardiologia* **48** (1966) 433–440.

6. S. Rodbard, A hydrodynamics mechanism for the autoregulation of flow. *Cardiologia* **48** (1966) 532–535.

7. R. D. Kamm, Bioengineering studies of periodic external compression as prophylaxis against deep vein thrombosis. Part I: Numerical studies. *J. Biomech. Engr.* **104** (1982) 87–95.

8. D. A. Olson, R. D. Kamm and A. H. Shapiro, Bioengineering studies of periodic external compression as prophylaxis against deep vein thrombosis. Part II: Experimental studies on a simulated leg. *J. Biomech. Engr.* **104** (1982) 96–104.

9. C. D. Bertram, C. J. Raymond and K. S. A. Butcher, Oscillations in a collapsed-tube analog of the brachial artery under a sphygmomanometer cuff. *J. Biomech. Engr.* **111** (1989) 185–191.

10. A. Ur and M. Gordon, Origin of Korotkoff sounds. *American Journal of Physiology* **218** (1970) 524–529.

11. N. Gavriely, Y. Palti, G. Alroy and J. B. Grotberg, Measurement and theory of wheezing breath sounds. *J. Appl. Physiol.* **57** (1984) 481–492.

12. N. Gavriely, T. R. Shee, D. W. Cugell and J. B. Grotberg, Flutter in flow-limited collapsible tubes: a mechanism for the generation of wheezes. *J. Appl. Physiol.* **66** (1989) 2251–2261.

13. G. S. Berke, D. C. Green, M. E. Smith, D. P. Arnstein, V. Honrubia, M. Natividad and W. A. Conrad, Experimental evidence in the in vivo canine for the collapsible tube model of phonation. *J. Acoust. Soc. Am.* **89** (1991) 1358–63.

14. J. B. Grotberg and O. E. Jensen, Biofluid mechanics in flexible tubes. *Annu. Rev. Fluid Mech.* **36** (2004) 121–147.

15. M. Heil and A. L. Hazel, Fluid–structure interaction in internal physiological flows. *Annu. Rev. Fluid Mech.* **43** (2011) 141–162.

16. F. P. Knowlton and E. H. Starling, The influence of variations in temperature and blood pressure on the performance of the isolated mammalian heart. *J. Physiol. London* **44** (1912) 206–219.

17. C. D. Bertram and J. Tscherry, The onset of flow-rate limitation and flow-induced oscillations in collapsible tubes. *J. Fluids Struct.* **22** (2006) 1029–1045.

18. C. D. Bertram, Experimental studies of collapsible tubes. In P. W. Carpenter and T. J. Pedley, editors, *Flow past highly compliant boundaries and in collapsible tubes*, chap. 3, pages 51–65, Springer (2003).

19. J. L. Bull, C. A. Reickert, S. Tredici, E. Komori, E. L. Frank, D. O. Brant, J. B. Grotberg and R. B. Hirschl, Flow limitation in liquid-filled lungs: effects of liquid properties. *J. Biomech. Engr.* **127** (2005) 630–636.

20. J.-M. Fullana and S. Zaleski, A branched one-dimensional model of vessel networks. *J. Fluid Mech.* **621** (2009) 183–204.

21. A. M. Venugopal, C. M. Quick, G. A. Laine and R. H. Stewart, Optimal postnodal lymphatic network structure that maximizes active propulsion of lymph. *Am. J. Physiol. Heart Circ. Physiol.* **296** (2009) H303–H309.

22. P. S. Stewart, S. L. Waters and O. E. Jensen, Local and global instabilities of flow in a flexible-walled channel. *Eur. J. Mech. B Fluids* **28** (2009) 541–557.

23. T. J. Pedley, Longitudinal tension variation in collapsible channels: A new mechanism for the breakdown of steady flow. *J. Biomech. Engr.* **114** (1992) 60–67.

24. X. Y. Luo, Z. Cai, W. G. Li and T. J. Pedley, The cascade structure of linear instability in collapsible channel flows. *J. Fluid Mech.* **600** (2008) 45–76.

25. H. F. Liu, X. Y. Luo and Z. X. Cai, Stability and energy budget of pressure-driven collapsible channel flows. *J. Fluid Mech.* **705** (2012) 348–370.

26. O. E. Jensen and M. Heil, High-frequency self-excited oscillations in a collapsible-channel flow. *J. Fluid Mech.* **481** (2003) 235–268.

27. R. J. Whittaker, S. L. Waters, O. E. Jensen, J. Boyle and M. Heil, The energetics of flow through a rapidly oscillating tube. I. General theory. *J. Fluid Mech.* **648** (2010a) 83–121.

28. R. J. Whittaker, M. Heil, J. Boyle, O. E. Jensen and S. L. Waters, The energetics of flow through a rapidly oscillating tube. II. Application to an elliptical tube. *J. Fluid Mech.* **648** (2010b) 123–153.

29. M. Heil and S. L. Waters, How rapidly oscillating collapsible tubes extract energy from a viscous mean flow. *J. Fluid Mech.* **601** (2008) 199–227.

30. C. D. Bertram, Flow-induced oscillation of collapsed tubes and airway structures. *Respir. Physiol. Neurobiol.* **163** (2008) 256–265.

31. R. J. Whittaker, M. Heil, O. E. Jensen and S. L. Waters, Predicting the onset of high-frequency self-excited oscillations in elastic-walled tubes. *Proc. R. Soc. Lond. Ser. A Math. Phys. Eng. Sci.* **466** (2010c) 3635–3657.

32. R. J. Whittaker, M. Heil, O. E. Jensen and S. L. Waters, A rational derivation of a tube law from shell theory. *Quart. J. Mech. Appl. Math.* **63** (2010d) 465–496.

33. W. Flügge, *Tensor analysis and Continuum Mechanics*. Springer (1972).

34. N. Søndergaard, Moving frames applied to shell elasticity. *J. Phys. A* **40** (2007) 5067–5081.

35. G. K. Batchelor, *An Introduction to Fluid Dynamics*. Camb. Univ. Press (1967), ISBN 0-521-66396-2.

36. M. Heil and A. L. Hazel, `oomph-lib` an *O*bject-*O*riented *M*ulti-*Ph*ysics finite-element *Lib*rary. In *Fluid-structure interaction*, vol. 53 of *Lect. Notes Comput. Sci. Eng.*, pages 19–49, Springer, Berlin (2006). Oomph-lib is available as open-source software at `http://www.oomph-lib.org/`.

37. M. Heil and J. Boyle, Self-excited oscillations in three-dimensional collapsible tubes: simulating their onset and large-amplitude oscillations. *J. Fluid Mech.* **652** (2010) 405–426.

APPENDIX A

Differential Operators and Functions in the PDE for $\eta(\tau, z)$

The differential operators $\mathscr{L}$, $\mathscr{K}$ and $\mathscr{J}$ and the function $C_p(\tau)$ that appear in (3.6) are

$$\begin{aligned}\mathscr{L}(\beta) \equiv\ & \frac{2}{c^2 \sinh 2\sigma_0} \frac{\partial^3 \beta}{\partial \tau^3} - \frac{6 \sin 2\tau}{c^2 \sinh 2\sigma_0 (\cosh 2\sigma_0 - \cos 2\tau)} \frac{\partial^2 \beta}{\partial \tau^2} \\ & - \frac{2(2\cos^2 2\tau + 8\cosh 2\sigma_0 \cos 2\tau - 9 - \cosh^2 2\sigma_0)}{c^2 \sinh 2\sigma_0 (\cosh 2\sigma_0 - \cos 2\tau)^2} \frac{\partial \beta}{\partial \tau} \\ & + \frac{6 \sin 2\tau\, (\cosh^2 2\sigma_0 - 5 + 4\cosh 2\sigma_0 \cos 2\tau)}{c^2 \sinh 2\sigma_0 (\cosh 2\sigma_0 - \cos 2\tau)^3} \beta\,, \end{aligned} \tag{A1}$$

$$\mathscr{K}(\eta) \equiv \frac{-2}{c^2 \sinh 2\sigma_0} \frac{\partial}{\partial \tau} \left(1 + \frac{\partial^2}{\partial \tau^2}\right) \eta\,, \tag{A2}$$

$$\begin{aligned}\mathscr{J}(\eta) \equiv\ & -\frac{\big(\cosh 2\sigma_0 - \cos 2\tau\big)^2}{\sinh^2 2\sigma_0} \frac{\partial^2 \eta}{\partial \tau^2} - \frac{3\big(\cosh 2\sigma_0 - \cos 2\tau\big) \sin 2\tau}{\sinh^2 2\sigma_0} \frac{\partial \eta}{\partial \tau} \\ & + \frac{2\sinh^2 2\sigma_0 + 3\sin^2 2\tau - \big(\cosh 2\sigma_0 - \cos 2\tau\big)^2}{\sinh^2 2\sigma_0} \eta\,, \end{aligned} \tag{A3}$$

$$C_p(\tau) = \frac{3 \sin 2\tau}{\sinh 2\sigma_0}\,. \tag{A4}$$

These match the definitions made by Whittaker *et al.* (**32**) for the related problem without wall inertia.

APPENDIX B

Proof That the Eigenfrequencies are Real

In this appendix, we prove that the eigenfrequencies ω of the system (5.3)–(5.8) always take non-zero real values. We start with the governing ODE (5.3) for $\tilde{p}$ in the flexible region ($z_1 < z < z_2$) of the tube, multiply it by the complex conjugate of $\tilde{p}''$ and integrate between z_1 and z_2:

$$\int_{z_1}^{z_2} \Big\{ k_2 \mathscr{F} \tilde{p}'''' \tilde{p}''^{\dagger} + (M\omega^2 k_2 - k_0)|\tilde{p}''|^2 - \omega^2 \tilde{p}''^{\dagger} \tilde{p} \Big\}\, \mathrm{d}z = 0, \tag{B1}$$

where $'$ denotes a derivative with respect to z and † represents the complex conjugate.

Using integration by parts on the first and last terms in the integrand, we obtain

$$\begin{aligned} -k_2 \mathscr{F} \int_{z_1}^{z_2} |\tilde{p}'''|^2\, \mathrm{d}z + (M\omega^2 k_2 - k_0) \int_{z_1}^{z_2} |\tilde{p}''|^2\, \mathrm{d}z & \\ -\omega^2 \left(\Big[\tilde{p}'^{\dagger} \tilde{p}\Big]_{z_1}^{z_2} - \int_{z_1}^{z_2} |\tilde{p}'|^2\, \mathrm{d}z \right) &= 0. \end{aligned} \tag{B2}$$

where the boundary contributions from the first term vanish because $\tilde{p}'' = 0$ at $z = z_1, z_2$ from (5.6).

We now perform an analogous procedure with the governing equation (5.4) in the rigid parts of the tube. Taking the complex conjugate of (5.4), multiplying by $\tilde{p}$, and integrating over each of the rigid sections, we have

$$\int_0^{z_1} \tilde{p}''^{\dagger}\tilde{p}\,\mathrm{d}z = 0, \qquad \int_{z_2}^{1} \tilde{p}''^{\dagger}\tilde{p}\,\mathrm{d}z = 0, \tag{B3}$$

Using integration by parts on these two integrals, we then obtain

$$\omega^2\int_0^{z_1} |\tilde{p}'|^2\,\mathrm{d}z - \omega^2\Big[\tilde{p}'^{\dagger}\tilde{p}\Big]_0^{z_1} = 0. \tag{B4}$$

$$\omega^2\int_{z_2}^{1} |\tilde{p}'|^2\,\mathrm{d}z - \omega^2\Big[\tilde{p}'^{\dagger}\tilde{p}\Big]_{z_2}^{1} = 0. \tag{B5}$$

We now sum equations (B2), (B4) and(B5). The boundary terms at $z = z_2, z_2$ cancel by virtue of the continuity conditions (5.5). Noting that $\tilde{p}'' = \tilde{p}''' = 0$ for $z \in (0, z_1)$ and $z \in (z_2, 1)$, we deduce

$$(M\omega^2 k_2 - k_0)\int_0^1 |\tilde{p}''|^2\,\mathrm{d}z - k_2\mathscr{F}\int_0^1 |\tilde{p}'''|^2\,\mathrm{d}z - \omega^2\Big[\tilde{p}'^{\dagger}\tilde{p}\Big]_0^1 + \omega^2\int_0^1 |\tilde{p}'|^2\,\mathrm{d}z = 0. \tag{B6}$$

Finally, we know that $\tilde{p} = 0$ at $z = 0$ from (5.7), and $\tilde{p}' = 0$ at $z = 1$ from (5.8), so the remaining boundary terms vanish. Rearranging (B6), we can then write

$$\omega^2 = \frac{\displaystyle\int_0^1 k_2\mathscr{F}|\tilde{p}'''|^2 + k_0|\tilde{p}''|^2\,\mathrm{d}z}{\displaystyle\int_0^1 |\tilde{p}'|^2 + k_2 M|\tilde{p}''|^2\,\mathrm{d}z}. \tag{B7}$$

The constants k_0 and k_2 are both strictly positive, while $\mathscr{F}$ and M are non-negative. Hence for any non-trivial solution $\tilde{p}$, the right-hand side of (B7) is real and strictly positive. Hence, ω must be real and non-zero.

APPENDIX C

The Oscillatory Energy in the Tube Wall

In this appendix, we derive an expression for $\tilde{\mathbb{E}}_s$, the period-averaged dimensionless oscillatory energy in the tube wall, including both the elastic and kinetic contributions.

C.1 *Rate of Working on the Tube Wall*

We start from the following (dimensional) expression for the rate of working on the tube wall due to pressure forces

$$\frac{\mathrm{d}E_s^*}{\mathrm{d}t^*} = \iint_{\text{Tube Wall}} p_{\text{tm}}^*\frac{\partial \mathbf{r}}{\partial t^*}\cdot\hat{\mathbf{n}}\,\mathrm{d}S. \tag{C1}$$

Here, E_s^* is the total dimensional energy in the tube wall as a result of work by the transmural pressure p_{tm}^*, $\mathrm{d}S$ is an element of the mid-plane of the tube wall, t^* is once again dimensional time, $\mathbf{r}$ is the position of the wall mid-plane in the deformed state, as defined in (2.19), and $\hat{\mathbf{n}}$ is a unit vector normal to the tube wall. The expression (C1) for the dimensional rate of working in the tube wall $\mathrm{d}E_s^*/\mathrm{d}t^*$ comes from integrating the product of the force from the transmural pressure and the normal component of the velocity of the tube wall, over the mid-plane of the tube wall.

Inserting the appropriate limits for the integration within (C1) and noting that p^*_{tm} is independent of τ, it is found that

$$\frac{\mathrm{d}E_s^*}{\mathrm{d}t^*} = \int_0^L p^*_{\mathrm{tm}} \int_0^{2\pi} \frac{\partial \mathbf{r}}{\partial t^*} \cdot \hat{\mathbf{n}}\, a h(\tau)\, \mathrm{d}\tau\, \mathrm{d}z^*. \tag{C2}$$

Now, to leading order, the area perturbation can be written as

$$A^* - A_0^* = \int_0^{2\pi} (\mathbf{r} - \mathbf{r}_0) \cdot \hat{\mathbf{n}}\, a h(\tau) \mathrm{d}\tau. \tag{C3}$$

By differentiating this relation with respect to t^* and then substituting the result into (C2), we obtain

$$\frac{\mathrm{d}E_s^*}{\mathrm{d}t^*} = \int_0^L p^*_{\mathrm{tm}} \frac{\partial A^*}{\partial t^*}\, \mathrm{d}z^*. \tag{C4}$$

The expression (C4) is now non-dimensionalized using the scalings (2.11) for the axial length and cross-sectional area, (2.14) for the transmural pressure, (2.17) for the energy and $t^* = Tt$ for time. Applying these scalings, the following is calculated

$$\frac{\mathrm{d}E_s}{\mathrm{d}t} = St^2 \ell^2 \int_{z_1}^{z_2} p_{\mathrm{tm}} \frac{\partial A}{\partial t}\, \mathrm{d}z, \tag{C5}$$

where E_s is the dimensionless energy in the tube wall. We note that $\partial A/\partial t = 0$ in the rigid regions of the tube and thus we only need to take the integral within (C5) over the region $z_1 < z < z_2$.

C.2 *Time-Dependent Energy in the Tube Wall*

We wish to integrate (C5) in order to obtain an expression for E_s. To achieve this, we first convert (C5) into an expression solely in terms of the area A, by using the tube law (3.9) to relate the transmural pressure p_{tm} to A. We obtain

$$\frac{\mathrm{d}E_s}{\mathrm{d}t} = \frac{St^2\ell^2}{A_0} \int_{z_1}^{z_2} \left(k_0 (A - A_0) \frac{\partial A}{\partial t} - k_2 \mathscr{F} \frac{\partial^2 A}{\partial z^2} \frac{\partial A}{\partial t} + k_2 M \frac{\partial^2 A}{\partial t^2} \frac{\partial A}{\partial t} \right) \mathrm{d}z. \tag{C6}$$

Using integration by parts on the second term in the integral (the boundary terms vanish as $\partial A/\partial t = 0$ at $z = z_1, z_2$) it can then be shown that

$$\frac{\mathrm{d}E_s}{\mathrm{d}t} = \frac{St^2\ell^2}{2A_0} \int_{z_1}^{z_2} \frac{\partial}{\partial t} \left[k_0 (A - A_0)^2 + k_2 \mathscr{F} \left(\frac{\partial A}{\partial z} \right)^2 + k_2 M \left(\frac{\partial A}{\partial t} \right)^2 \right] \mathrm{d}z. \tag{C7}$$

Integrating both sides with respect to t, we find

$$E_s = \frac{St^2\ell^2}{2A_0} \int_{z_1}^{z_2} \left[k_0 (A - A_0)^2 + k_2 \mathscr{F} \left(\frac{\partial A}{\partial z} \right)^2 + k_2 M \left(\frac{\partial A}{\partial t} \right)^2 \right] \mathrm{d}z + C, \tag{C8}$$

where C is some constant dependent on the steady deformation of the tube wall.

C.3 *Decomposition into Steady and Oscillatory Components*

We now recall the decomposition (2.16) of the cross-sectional area $A(z,t)$

$$A(z,t) = A_0 + \frac{1}{\alpha^2 \ell St} \bar{A}(z) + \Delta(t)\, \mathrm{Re}\Big(\tilde{A}(z) e^{\mathrm{i}\omega t} \Big). \tag{C9}$$

Substituting this into (C8), we obtain

$$E_s = \frac{St^2\ell^2}{2A_0}\int_{z_1}^{z_2} k_0\left[\frac{1}{\alpha^2\ell St}\bar{A} + \Delta\,\mathrm{Re}\left(\tilde{A}e^{\mathrm{i}\omega t}\right)\right]^2 - \Delta^2 M\omega^2 k_2\left[\mathrm{Re}\left(\tilde{A}e^{\mathrm{i}\omega t}\right)\right]^2 + k_2\mathscr{F}\left[\frac{1}{\alpha^2\ell St}\frac{\partial\bar{A}}{\partial z} + \Delta\,\mathrm{Re}\left(\frac{\partial\tilde{A}}{\partial z}e^{\mathrm{i}\omega t}\right)\right]^2 \mathrm{d}z + C. \tag{C10}$$

We now evaluate the time-averaged energy $\mathbb{E}_s$ over a single oscillation, defined by

$$\mathbb{E}_s = \langle E_s\rangle = \frac{\omega}{2\pi}\int_{t_0}^{t_0+\frac{2\pi}{\omega}} E_s\,\mathrm{d}t, \tag{C11}$$

where it is assumed that the variation in Δ over the interval $(t_0, t_0+\frac{2\pi}{\omega})$ is negligible. It can be shown that if a function $\mathbb{A}(z,t)$ has the form $\mathbb{A}(z,t) = \bar{\mathbb{A}}(z) + \mathrm{Re}(\tilde{\mathbb{A}}(z)e^{\mathrm{i}\omega t})$, then

$$\langle\mathbb{A}^2\rangle = \bar{\mathbb{A}}^2 + \frac{1}{2}|\tilde{\mathbb{A}}|^2. \tag{C12}$$

Using this property, we take the time-average of (C10) to obtain

$$\mathbb{E}_s = \frac{St^2\ell^2}{2A_0}\int_{z_1}^{z_2} k_0\left(\frac{1}{\alpha^4\ell^2 St^2}\bar{A}^2 + \frac{\Delta^2}{2}\left|\tilde{A}\right|^2\right) + \frac{\Delta^2 M\omega^2 k_2}{2}\left|\tilde{A}\right|^2 + k_2\mathscr{F}\left(\frac{1}{\alpha^4\ell^2 St^2}\left(\frac{\partial\bar{A}}{\partial z}\right)^2 + \frac{\Delta^2}{2}\left|\frac{\partial\tilde{A}}{\partial z}\right|^2\right)\mathrm{d}z + C. \tag{C13}$$

Hence, $\mathbb{E}_s$ may be decomposed into components due to the steady and oscillatory area changes of the tube. Thus, the period-averaged dimensionless energy $\tilde{\mathbb{E}}_s$ in the tube wall due to the oscillations is given by

$$\tilde{\mathbb{E}}_s = \frac{\Delta^2 St^2\ell^2}{4A_0}\int_{z_1}^{z_2}\left((k_0 + M\omega^2 k_2)\left|\tilde{A}\right|^2 + k_2\mathscr{F}\left|\frac{\partial\tilde{A}}{\partial z}\right|^2\right)\mathrm{d}z. \tag{C14}$$

It is convenient to express $\tilde{\mathbb{E}}_s$ in terms of $\tilde{p}$ rather than $\tilde{A}$. Using (4.7) we obtain

$$\tilde{\mathbb{E}}_s = \frac{\Delta^2 St^2 A_0\ell^2}{4\omega^4}\int_{z_1}^{z_2}\left((k_0 + M\omega^2 k_2)\tilde{p}''\tilde{p}''^{\dagger} + k_2\mathscr{F}\tilde{p}'''\tilde{p}'''^{\dagger}\right)\mathrm{d}z, \tag{C15}$$

where $'$ denotes a derivative with respect to z and † denotes the complex conjugate.

C.4 *Simplification of the expression for* $\tilde{\mathbb{E}}_s$

The expression (C15) for $\tilde{\mathbb{E}}_s$ could be used directly in the energy budget in §7. However, a further simplification is possible to reduce the number of derivatives of $\tilde{p}$ required.

First, we use integration by parts on the final term in the integrand in (C15). The boundary terms vanish as $\tilde{p}'' = 0$ at $z = z_1, z_2$, and we obtain

$$\tilde{\mathbb{E}}_s = \frac{\Delta^2 St^2 A_0\ell^2}{4\omega^4}\int_{z_1}^{z_2}\left((k_0 + M\omega^2 k_2)\tilde{p}''\tilde{p}''^{\dagger} - k_2\mathscr{F}\tilde{p}''''\tilde{p}''^{\dagger}\right)\mathrm{d}z. \tag{C16}$$

We now use the governing ODE (5.3) to replace $\tilde{p}''''$ by terms involving lower-order derivatives of $\tilde{p}$. The terms involving k_0 cancel, and we find that

$$\tilde{\mathbb{E}}_s = \frac{\Delta^2 St^2 A_0\ell^2}{4\omega^2}\int_{z_1}^{z_2}\left(2Mk_2\tilde{p}''\tilde{p}''^{\dagger} - \tilde{p}\tilde{p}''^{\dagger}\right)\mathrm{d}z. \tag{C17}$$

By integrating the second term in the integrand of (C17) by parts, we find that

$$\tilde{\mathbb{E}}_s = \frac{\Delta^2 St^2 A_0 \ell^2}{4\omega^2} \left\{ \int_{z_1}^{z_2} \left(\left|\tilde{p}'\right|^2 + 2Mk_2 \left|\tilde{p}''\right|^2 \right) \mathrm{d}z - \left[\tilde{p}\tilde{p}'^{\dagger} \right]_{z=z_1}^{z=z_2} \right\}. \tag{C18}$$

Noting the boundary conditions (5.6)–(5.8) at $z = z_1, z_2$ together with the solutions (6.1)–(6.2) for $\tilde{p}$ in $(0, z_1)$ and $(z_2, 1)$, we can re-express the boundary terms as

$$-\left[\tilde{p}\tilde{p}'^{\dagger} \right]_{z=z_1}^{z=z_2} = z_1 \left|\tilde{p}'\right|^2 \Big|_{z=z_1} = \int_0^{z_1} \left|\tilde{p}'\right|^2 \mathrm{d}z. \tag{C19}$$

Then since $\tilde{p}'' = 0$ for $z \in (0, z_1)$ and $\tilde{p}' = \tilde{p}'' = 0$ for $z \in (z_2, 1)$, we can re-write (C18) a single integral over the whole domain, thus

$$\tilde{\mathbb{E}}_s = \frac{\Delta^2 St^2 A_0 \ell^2}{4\omega^2} \int_0^1 \left(\left|\tilde{p}'\right|^2 + 2Mk_2 \left|\tilde{p}''\right|^2 \right) \mathrm{d}z. \tag{C20}$$